Patterson maps and subsequent cycles of least-squares refinement and calculation of difference Fourier maps.

{(OEOP)$Fe^{III}Br_2$}. There is disorder in the oxygen atom location, and carbon atom C(1) was refined as coincident with O(1). Hydrogen atoms were located on a difference map and fixed at ideal geometries for subsequent cycles of least-squares refinement. A difference map showed a peak with intensity of 0.5 e/Å^3 that was 1.1 Å from C(1). This was added to the model of the structure at fixed, ideal geometry, and four more cycles of full-matrix least-squares refinement were run. The unit cell contains two molecules of diethyl ether which are disordered across a mirror plane and a 2-fold axis. After many different models were tried, a group of five atoms was selected that best approximate the diethyl ether. The positional parameters for this molecule were ultimately fixed, the occupancies were set at 0.25, and only isotropic thermal parameters were refined. During final stages of refinement, all the remaining nonhydrogen atoms were assigned anisotropic thermal parameters. The largest peak in the final difference map is 2.26 Å from Br and has an electron density of 1.2 e/Å^3.

{(OEOP)$Fe^{II}Cl$}. There is disorder in the occupancy at the sites of O(1) and C(10). The arrangement shown in Figure 8 has a computed occupancy of 55(3)%. The other arrangement interchanges O(1) and C(10).

Instrumentation. ^{1}H NMR spectra were recorded on a General Electric QE-300 FT NMR spectrometer operating in the quadrature mode (^{1}H frequency is 300 MHz). The spectra were collected over a 50-kHz bandwidth with 16K data points and a 5-μs 45° pulse. For a typical spectrum, between 1000 and 5000 transients were accumulated with a 50-ms delay time. The signal-to-noise ratio was improved by apodization of the free inducting decay. Electronic spectra were obtained using a Hewlett-Packard diode array spectrometer.

The MCOSY spectra were obtained as described previously[22] after a standard 1D reference spectrum was collected. The 2D spectra were collected by the use of 1024 points in t_2 that were collected over the bandwidth necessary to include the desired resonances with 512 t_1 blocks and 1024 scans per block. These were zero filled to 1024 t_2 × 1024 t_1. All experiments included four dummy scans prior to collection of the first block.

Acknowledgment. We thank the NIH (GM-26226) for financial support.

Supplementary Material Available: Tables of atomic positional parameters, bond distances, bond angles, anisotropic thermal parameters, and crystal data for {(OEOP)$Fe^{III}Br_2$} and {(OEOP)$Fe^{II}Cl$} (17 pages); observed and calculated structure factors (16 pages). Ordering information is given on any current masthead page.

η^2-Coordination and C–F Activation of Hexafluorobenzene by Cyclopentadienylrhodium and -iridium Complexes

Simon T. Belt,[1a] Madeleine Helliwell,[1a] William D. Jones,[1b] Martin G. Partridge,[1a] and Robin N. Perutz*,[1a]

Contribution from the Departments of Chemistry, University of York, Heslington, York, YO1 5DD, U.K., and University of Rochester, Rochester, New York 14627.
Received August 17, 1992

Abstract: The photochemical reaction of (η^5-C_5R_5)$Rh(PMe_3)(C_2H_4)$ (R = H, Me) with hexafluorobenzene yields (η^5-C_5R_5)$Rh(PMe_3)(\eta^2$-$C_6F_6)$. The structure of (η^5-C_5H_5)$Rh(PMe_3)(\eta^2$-$C_6F_6)$ has been determined crystallographically (a = 10.533, b = 11.271, c = 13.074 Å, orthorhombic, space group *Pnma*, Z = 4). The C_6F_6 ligand is bound through two carbons and is distorted to generate a planar C_6F_4 unit with the two remaining C–F bonds at 43.8° to the plane. Several reactions of (η^5-C_5H_5)$Rh(PMe_3)(\eta^2$-$C_6F_6)$ are reported which yield (η^5-C_5H_5)$Rh(PMe_3)$L or (η^5-C_5H_5)$Rh(PMe_3)$(X)Y (L = CO, PPh_3; X = Ph, Si^iPr_3, Y = H; X = Y = Cl) either photochemically or thermally. The extended photolysis of (η^5-C_5Me_5)$Rh(PMe_3)(\eta^2$-$C_6F_6)$ generates a second product assigned as (η^5-C_5Me_5)$Rh(PMe_3)(C_6F_5)$F. The chlorination of this complex yields (η^5-C_5Me_5)$Rh(PMe_3)(C_6F_5)$Cl. The crystal structure of the latter (a = 14.129 (4), b = 9.610 (7), c = 30.320 (5) Å, β = 94.88 (5)°, monoclinic, space group $C2/c$, Z = 8) reveals a sterically congested molecule with the C_6F_5 group lying in a plane at an angle of 20° to the plane of the C_5Me_5 ring. The isolation and subsequent photolysis of (η^5-C_5Me_5)$Rh(PMe_3)(\eta^2$-$C_6F_6)$ in C_6F_6 also generates the C–F activation products. The thermal reaction of (η^5-C_5Me_5)$Rh(PMe_3)(C_6H_5)$H in C_6F_6 yields only the η^2-C_6F_6 complex. (η^5-C_5Me_5)$Rh(PMe_3)(\eta^2$-$C_6F_6)$. The results indicate that C_6F_6 reacts with the (η^5-C_5Me_5)$Rh(PMe_3)$ fragment in two sequential steps, with the formation of (η^5-C_5Me_5)$Rh(PMe_3)(\eta^2$-$C_6F_6)$ required before C–F insertion occurs. The photolysis of (η^5-C_5H_5)$Ir(PMe_3)H_2$ in C_6F_6 generates (η^5-C_5H_5)$Ir(PMe_3)(\eta^2$-$C_6F_6)$ and (η^5-C_5H_5)$Ir(PMe_3)(C_6F_5)$H concurrently. ^{2}H labeling studies show that the hydride ligand of the product derives from the hydride of the precursor. This CF insertion reaction is postulated to proceed via a ring slip or hydrogen-transfer mechanism, independently of the formation of (η^5-C_5H_5)$Ir(PMe_3)(\eta^2$-$C_6F_6)$. Irradiation of (η^5-C_5R_5)$Rh(PMe_3)(\eta^2$-$C_6F_6)$ (R = H, Me) in Ar matrices at 12 K results in two competing photochemical reactions: the first yields C_6F_6 and $CpRh(PMe_3)$ and the second generates the C–F insertion product. (η^5-C_5R_5)$Rh(PMe_3)(C_6F_5)$F. The expelled C_6F_6 and the insertion products are identified by their characteristic IR spectra. Dissociation of C_6F_6 is far more important for the (η^5-C_5H_5) than for the (η^5-C_5Me_5) complex. When (η^5-C_5H_5)-$Rh(PMe_3)(\eta^2$-$C_6F_6)$ is photolyzed in N_2 matrices, the $CpRh(PMe_3)$ fragment is trapped to form (η^5-C_5H_5)$Rh(PMe_3)(N_2)$. In CO-doped argon matrices, trapping results in formation of (η^5-C_5H_5)$Rh(PMe_3)$CO, and formation of the insertion product is suppressed.

Introduction

Partial coordination of arenes to transition metals (i.e., η^2- or η^4-coordination) may be considered either as a step toward full (η^6) coordination (eqs 1 and 2) or as a step toward oxidative addition (eq 3). The coordination/decoordination process may be induced by removal/addition of other ligands (eq 1), by irradiation, or by electron transfer (eq 2).[2] If we are to arrest these reactions at the η^2- or η^4-arene stage, there are three parameters

(1) (a) University of York. Present address of S.T.B.: Department of Chemistry, University of Ottawa, Ottawa, Ontario, Canada K1N 6N5. Present address of M.H.: Department of Chemistry, University of Manchester, Manchester, M13 9PL, U.K. (b) University of Rochester.

(2) Pierce, D. T.; Geiger, W. E. *J. Am. Chem. Soc.* **1989**, *111*, 7636. Bowyer, W. J.; Geiger, W. E. *J. Electroanal. Chem.* **1988**, *239*, 253; *J. Am. Chem. Soc.* **1985**, *107*, 5657. Bowyer, W. J.; Merkert, J. W.; Geiger, W. E.; Rheingold, A. L. *Organometallics* **1989**, *8*, 191.

0002-7863/93/1515-1429$04.00/0

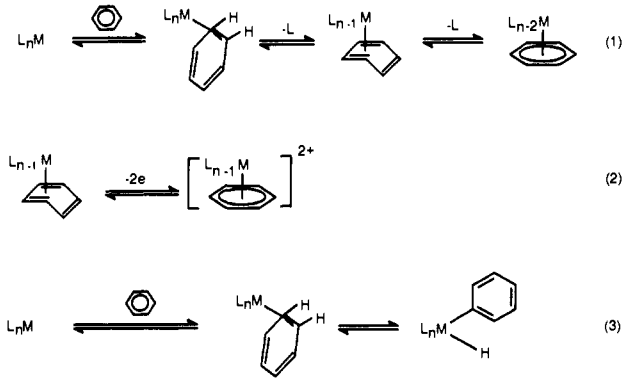

of particular importance: (i) the choice of metal and its electron configuration, (ii) the choice of arene, and (iii) the choice of ancillary ligands.

(i) Metal and Electron Configuration. Examples of the η^2-coordination mode used to be thought typical for the d^{10} systems Cu^I and Ag^I,[3] not prone to oxidative addition, and unsuitable for η^6-coordination. The only exception was the d^{10} Pt complex $Pt(PEt_3)_2[\eta^2\text{-}C_6(CF_3)_6]$,[4] which seemed to be a curiosity considering the ability of Pt^0 to undergo oxidative addition. In recent years, Harman and Taube[5] showed that the d^6 $[Os(NH_3)_5]^{2+}$ fragment is also suitable for η^2-coordination—this fragment is again not prone to oxidative addition.[6]

(ii) Choice of Arene. The choice of arene for η^2- or η^4-coordination has been subjected to only limited analysis. However, it has been shown that η^2- or η^4-coordination is more favorable for polycyclic aromatics over monocyclics because of the reduced loss of resonance stabilization on coordination.[7] The effect of substituents on the rate of arene dissociation from $[Os(NH_3)_5(\eta^2\text{-arene})]^{2+}$ has also been reported.[5c]

(iii) Choice of Ancillary Ligands. We have shown that oxidative addition of arenes will be favored over η^2-coordination (eq 3) by electron-donating ligands just as in the case of the metal dihydride/metal (dihydrogen) equilibria.[8] The effect of methyl substitution of the arene and cyclopentadienyl rings on redox equilibria (eq 2) has been reported.[2]

Our discovery that C_6F_6 is a good ligand for η^2- and η^4-coordination highlighted several aspects of control of coordination.[9] Firstly, we showed that d^8 half-sandwich complexes can support stable η^2-arene complexes even though arenes with C–H bonds typically undergo oxidative addition to such complexes. Thus $CpRh(PMe_3)(\eta^2\text{-}C_6F_6)$ ($Cp = \eta^5\text{-}C_5H_5$) is an isolable complex, whereas $CpRh(PMe_3)(\eta^2\text{-}C_6H_6)$ is a reactive intermediate with a millisecond lifetime which is unstable with respect to the corresponding phenyl hydride.[10] Secondly, we showed that the geometry of the $\eta^2\text{-}C_6F_6$ ligand in this complex and in $CpIr(C_2H_4)(\eta^2\text{-}C_6F_6)$ resembles that of a coordinated alkene.[9] The corollary of this observation is that such uncharged η^2-arene complexes are favored by electron-withdrawing substituents just as has been observed for alkene complexes.[9,11] In contrast η^6-arene complexes are favored by electron-donating substituents.[12] Seen in this light, $Pt(PEt_3)_2[\eta^2\text{-}C_6(CF_3)_6]$ was the first example[4] in which the η^2-geometry was stabilized by an electron-withdrawing arene.

Despite numerous postulates of η^2-arene complexes as reaction intermediates and the isolation of the osmium complexes, crystallographic characterizations of $M(\eta^2$-monocyclic arene) complexes are very limited.[3,4] Other structures involve either polycyclic arenes imposing different structural constraints as in $Cp^*Rh(PMe_3)(\eta^2$-phenanthrene)[7g] ($Cp^* = \eta^5\text{-}C_5Me_5$) or more than one metal as in $[Cp^*Re(CO)_2]_2(\mu\text{-}\eta^2\text{-}\eta^2\text{-}C_6H_6)$.[13]

The rhodium complexes also offer opportunities for variation of ancillary ligands. While $CpRh(PMe_3)(\eta^2\text{-}C_6F_6)$ showed no signs of C–F oxidative addition, we found that C–F activation is possible with the pentamethylcyclopentadienyl analogue.[14] The first reports of C–F bond activation involved the intramolecular activation of C–F bonds of pendant C_6F_5 groups.[15] Recently, reports have appeared of lanthanides reacting with C_6F_6.[16,17] At the same time as we reported C–F activation by $Cp^*Rh(PMe_3)(C_2H_4)$, Milstein et al. showed that the thermolysis of $MeIr(PEt_3)_3$ in C_6F_6 at 60 °C brings about formation of $(Et_3P)_2Ir(PEt_2F)(C_6F_5)$.[18] The mechanism is postulated to involve electron transfer followed by attack by $[C_6F_6]^{\bullet-}$ on the grounds that benzene is unreactive in this system (unlike that described here). Very recently it has been shown that $Pt(dtbpm)(CH_2CMe_3)H$ (dtbpm = $Bu^t_2PCH_2PBu^t_2$) reacts thermally with C_6F_6 to yield $Pt(dtbpm)(C_6F_5)F$.[19]

In this article we report in full the characterization of $CpRh(PMe_3)(\eta^2\text{-}C_6F_6)$ and its Cp^* analogue. We compare their reactivities to one another and contrast the reactivity of the $Cp^*Rh(PMe_3)$ and $CpIr(PMe_3)$ systems toward C_6F_6. We show that the $Cp^*Rh(PMe_3)$ and $CpIr(PMe_3)$ fragments are capable of C–F activation in different ways. We also examine the photochemical reactivity of $CpRh(PMe_3)(\eta^2\text{-}C_6F_6)$ and its Cp^* analogue in low-temperature matrices and show that both complexes undergo C–F insertion under these conditions as well as photodissociation of C_6F_6.

Experimental Section

Synthetic Methods. The syntheses were carried out with standard Schlenk methods under an argon atmosphere. The solutions, made up in small Pyrex ampules fitted with polytetrafluoroethylene stopcocks, were degassed with three freeze–pump–thaw cycles and then back-filled with argon before irradiation with an Applied Photophysics 250-W high-pressure mercury arc. Hexafluorobenzene (99.9%) from Aldrich was distilled under argon and stored over molecular sieves (grade 4A) prior to use. Deuterated solvents were obtained from Goss and dried over potassium benzophenone ketyl. Microanalyses were performed by Butterworth Laboratories.

(3) (a) Turner, R. W.; Amma, E. L. *J. Am. Chem. Soc.* **1966**, *88*, 3243. (b) Turner, R. W.; Amma, E. L. *J. Am. Chem. Soc.* **1966**, *88*, 1877.
(4) (a) Browning, J.; Green, M.; Spencer, J. L.; Stone, F. G. A. *J. Chem. Soc., Dalton Trans.* **1974**, 97. (b) Cobbledick, R. E.; Einstein, F. W. B. *Acta Crystallogr.* **1978**, *B34*, 1849. (c) Browning, J.; Penfold, B. R. *J. Cryst. Mol. Struct.* **1974**, *4*, 335.
(5) (a) Harman, W. D.; Taube, H. *Inorg. Chem.* **1987**, *26*, 2917. (b) Harman, W. D.; Taube, H. *J. Am. Chem. Soc.* **1988**, *110*, 5403. (c) Harman, W. D.; Sekine, M.; Taube, H. *J. Am. Chem. Soc.* **1988**, *110*, 5725.
(6) Elian, M.; Hoffmann, R. *Inorg. Chem.* **1975**, *14*, 1058.
(7) (a) Jonas, K. *J. Organomet. Chem.* **1974**, *78*, 273. (b) Brauer, D. J.; Krüger, C. *Inorg. Chem.* **1977**, *16*, 884. (c) Albright, J. O.; Datta, S.; Dezube, B.; Kouba, J. K.; Marynick, D. S.; Wreford, S. S.; Foxman, B. M. *J. Am. Chem. Soc.* **1979**, *101*, 611. (d) Hull, J. W.; Gladfelter, W. L. *Organometallics* **1984**, *3*, 605. (e) Jonas, K. *Pure Appl. Chem.* **1990**, *62*, 1169. (f) Jonas, K. *J. Organomet. Chem.* **1990**, *400*, 165. (g) Jones, W. D.; Dong, L. *J. Am. Chem. Soc.* **1989**, *111*, 8722.
(8) Kubas, G. J. *Acc. Chem. Res.* **1988**, *21*, 120.
(9) Bell, T. W.; Helliwell, M.; Partridge, M. G.; Perutz, R. N. *Organometallics* **1992**, *11*, 1911.
(10) Belt, S. T.; Duckett, S. B.; Helliwell, M.; Perutz, R. N. *J. Chem. Soc., Chem. Commun.* **1989**, 928.
(11) Guggenberger, L. J.; Cramer, R. J. *J. Am. Chem. Soc.* **1972**, *94*, 3799. Mingos, D. M. P. In *Comprehensive Organometallic Chemistry*; Wilkinson, G., Stone, F. G. A., Abel, E. W., Eds.; Pergamon Press: Oxford, UK, 1982; Vol. 3, p 1 and references therein.
(12) Muetterties, E. L.; Bleeke, J. R.; Sievert, A. C. *J. Organomet. Chem.* **1979**, *178*, 197. Zimmerman, C. L.; Shaner, S. L.; Roth, S. A.; Willeford, B. R. *J. Chem. Res., Synop.* **1980**, 108.
(13) van der Heijden, H.; Orpen, A. G.; Pasman, P. *J. Chem. Soc., Chem. Commun.* **1985**, 1576.
(14) Jones, W. D.; Partridge, M. G.; Perutz, R. N. *J. Chem. Soc., Chem. Commun.* **1991**, 264.
(15) Richmond, T. G.; Osterberg, C. E.; Arif, A. M. *J. Am. Chem. Soc.* **1987**, *109*, 8091. Anderson, C. M.; Puddephatt, R. J.; Ferguson, G.; Lough, A. J. *J. Chem. Soc., Chem. Commun.* **1989**, 1297. Crespo, M.; Martinez, M.; Sales, J. *J. Chem. Soc., Chem. Commun.* **1992**, 822. Lucht, B. L.; Poss, M. J.; King, M. A.; Richmond, T. G. *J. Chem. Soc., Chem. Commun.* **1991**, 400. Anderson, C. M.; Crespo, M.; Ferguson, G.; Lough, A. J.; Puddephatt, R. J. *Organometallics* **1992**, *11*, 171.
(16) Burns, C. J.; Andersen, R. A. *J. Chem. Soc., Chem. Commun.* **1989**, 136.
(17) Watson, P. L.; Tulip, T. H.; Williams, I. *Organometallics* **1990**, *9*, 1999.
(18) Blum, O.; Frolow, F.; Milstein, D. *J. Chem. Soc., Chem. Commun.* **1991**, 258.
(19) Hoffmann, P.; Unfried, G. *Chem. Ber.* **1992**, *125*, 659.

Table I. Crystallographic Parameters for the Structures of $CpRh(PMe_3)(\eta^2\text{-}C_6F_6)$ and $Cp^*Rh(PMe_3)(C_6F_5)Cl$

	$CpRh(PMe_3)(\eta^2\text{-}C_6F_6)$	$Cp^*Rh(PMe_3)(C_6F_5)Cl$
empirical formula	$C_{14}H_{14}F_6PRh$	$C_{19}H_{24}F_5PClRh$
color and habit	orange block	orange block
cryst size/mm	0.8 × 0.6 × 0.5	0.2 × 0.32 × 0.36
cryst system	orthorhombic	monoclinic
space group	*Pnma*	C_2/c
cell dimens		
a/Å	10.533	14.129 (4)
b/Å	11.271	9.610 (7)
c/Å	13.074	30.320 (5)
β/deg		94.88 (4)
V/Å^3	1552.11	4102 (5)
Z	4	8
formula mass, amu	430.15	516.72
density (calcd)/Mg m^{-3}	1.84	1.67
F(000)	847.99	2080
diffractometer	Hilger and Watts	Enraf-Nonius CAD4
radiation	Mo Kα	Mo Kα
wavelength/Å	0.7107	0.71069
temp/K	298	198
2θ max/deg ($\omega/2\theta$ mode)	54°	49.9°
scan type	$\omega/2\theta$	$\omega/2\theta$
index range	h, 13 to −13; k, 0 to 14; l, 0 to 16	h, 0 to 16; k, 0 to 11; l, −36 to 36
scan speed	0.5–4 s step^{-1}	2–15° min^{-1}
scan range		0.7 + 0.35 tan θ
no. of rflns measd	4396	4579
no. of indep rflns	1685 (R_{int} = 2%)	4280
no. of obsd reflns	1507 [$I > 2\sigma(I)$]	2429 [$I > 3\sigma(I)$]
corrns applied	R_{int} = 1%. Lorentz and polarization absorption corrections with three ψ scans	differential absorption
solution	direct methods and difference Fourier	Patterson
refinement	full-matrix least-squares	full-matrix least-squares
H atoms	Cp H's from difference map; PMe_3 hydrogens not included	in calcd positions from electron density map
weighting scheme	$w^{-1} = \sigma^2(F_o) + 0.003566F_o^2$	$w^{-1} = [\sigma^2(F_o) + \rho(F_o^2)]^{0.5}$
no. of variables	129	244
final R (obsd data)	R = 3.75%, R_w = 4.97%	R = 3.6%, R_w = 4.5%
goodness of fit		1.18
largest diff peak/e Å^{-3}	0.62	0.60

Spectroscopic Methods. NMR spectra were measured on a Bruker MSL 300 instrument in C_6D_6 referenced as follows: ^1H relative to C_6D_5H at δ 7.13; ^{31}P relative to an external sample of 85% H_3PO_4; ^{19}F relative to external $CFCl_3$. Mass spectra were recorded on a VG Autospec. Infrared spectra were recorded on a Mattson Sirius FTIR or a Perkin-Elmer 580 spectrometer.

Crystallographic Methods. (1) $CpRh(PMe_3)(\eta^2\text{-}C_6F_6)$. The structure of $CpRh(PMe_3)(\eta^2\text{-}C_6F_6)$ was determined in York on an upgraded Hilger and Watts four-circle diffractometer with filtered Mo Kα radiation, following preliminary measurements with a precession camera. Accurate cell dimensions were obtained from 30 centered reflections. Conditions for data collection and refinement together with lattice parameters are listed in Table I. Absorption corrections were applied using the empirical method of North et al.[20] and Lp corrections were applied. MULTAN87[21] was used to find the rhodium position. The remaining atoms were located by subsequent difference Fourier maps with the aid of SHELX76.[22] The measurement of four standard reflections in every 200 revealed no signs of crystal decay. The final structure was refined with conventional Fourier synthesis in SHELX. Anisotropic thermal parameters were refined for all non-hydrogen atoms. Some hydrogen atoms were found in successive difference Fourier maps and refined isotropically.

The PMe_3 group was disordered, with the best model for this group being obtained by refining two positions for each methyl carbon atom. The second position was obtained from the first by reflection in the mirror plane parallel to the xz plane and at $y = {}^1/_4$. Each position was given an occupancy of 0.5. Temperature factors in this group were correspondingly high. The final refinement of the 129 variable parameters converged with R = 0.0375 and R_w = 0.0497. Interatomic distances between non-hydrogen atoms and selected bond angles are given in Table II. Full crystallographic data and a packing diagram are given in the supplementary material (Tables VII–VIII and Figure 5). Atomic scattering factors were taken from International Tables.[23] Plots were generated using PLUTO.[24]

Table II. Interatomic Distances of Non-Hydrogen Atoms and Selected Bond Angles in $CpRh(PMe_3)(\eta^2\text{-}C_6F_6)$

	Interatomic Distances/Å		
C(1)–C(2)	1.426 (7)	C(7)–C(7)′	1.397 (12)
C(2)–C(3)	1.411 (8)	C(7)–C(8)	1.473 (8)
C(3)–C(3)′	1.376 (11)	C(8)–C(9)	1.331 (8)
		C(9)–C(9)′	1.354 (12)
Rh–P	2.283 (2)	Rh–C(1)	2.238 (6)
Rh–C(7)	2.058 (4)	Rh–C(2)	2.292 (4)
		Rh–C(3)	2.264 (4)
P–C(4)	1.847 (9)	C(7)–F(7)	1.384 (5)
P–C(5)	1.862 (14)	C(8)–F(8)	1.348 (7)
P–C(6)	1.837 (20)	C(9)–P(9)	1.357 (6)
C(4)–C(4)′	1.162 (32)[a]	C(5)–F(7)′	2.773 (17)
C(5)–C(6)′	0.974 (30)[a]	C(6)–F(7)	3.109 (23)
	Bond Angles/deg		
Ph–Rh–C(7)	95.5 (0.1)	Rh–P–C(4)	113.0 (0.4)
P–Rh–C(1)	156.9 (0.2)	Rh–P–C(5)	120.2 (0.6)
P–Rh–C(2)	127.7 (0.2)	Rh–P–C(6)	112.8 (0.6)
P–Rh–C(3)	97.4 (0.1)	C(4)–P–C(5)	97.7 (0.8)
Rh–C(7)–F(7)	120.9 (0.3)	C(5)–P–C(6)	104.6 (1.3)
Rh–C(7)–C(8)	116.2 (0.3)	C(4)–P–C(6)	106.8 (1.1)
C(7)–Rh–C(7)′	39.7 (0.3)	C(8)–C(9)–F(9)	120.3 (0.6)
C(1)–C(2)–C(3)	106.7 (0.4)	C(9)–C(8)–F(8)	122.6 (0.6)
C(7)–C(8)–C(9)	120.8 (0.5)	C(7)–C(8)–F(8)	116.6 (0.6)
		C(8)–C(7)–F(7)	109.9 (0.5)

[a] These are the distances between the positions of the phosphine carbon atoms, each with 50% occupancy.

(20) North, A. C. T.; Phillips, D. C.; Mathews, F. A. *Acta Crystallogr.* **1968**, *A24*, 35.
(21) MULTAN87: Debaerdemaeker, T.; Tate, C.; Woolfson, M. M. *Acta Crystallogr.* **1985**, *A41*, 286.
(22) Sheldrick, G. M. *SHELX76, A Program system for crystal structure determinations*; University of Cambridge: Cambridge, England, 1976.
(23) Cramer, D. T. *International Tables for Crystallography*; Kynoch Press: Birmingham, UK, 1974; Vol. IV.

Table III. Interatomic Distances of Non-Hydrogen Atoms and Selected Angles in $Cp^*Rh(PMe_3)(C_6F_5)Cl$

	Interatomic Distances/Å		
C(1)–C(2)	1.463 (8)	C(1)–C(6)	1.497 (8)
C(1)–C(5)	1.402 (8)	C(2)–C(7)	1.503 (9)
C(2)–C(3)	1.398 (8)	C(3)–C(8)	1.500 (8)
C(3)–C(4)	1.441 (8)	C(4)–C(9)	1.499 (8)
C(4)–C(5)	1.440 (8)	C(5)–C(10)	1.498 (8)
Rh–Cl	2.411 (2)	C(11)–C(12)	1.371 (8)
Rh–P	2.282 (2)	C(12)–C(13)	1.374 (8)
Rh–C(11)	2.070 (5)	C(13)–C(14)	1.361 (9)
P–C(17)	1.807 (7)	C(14)–C(15)	1.366 (9)
P–C(18)	1.804 (7)	C(15)–C(16)	1.378 (8)
P–C(19)	1.803 (7)	C(16)–C(11)	1.387 (8)
Rh–C(1)	2.203 (6)	F(1)–C(12)	1.373 (7)
Rh–C(2)	2.223 (6)	F(2)–C(13)	1.350 (7)
Rh–C(3)	2.219 (5)	F(3)–C(14)	1.349 (6)
Rh–C(4)	2.131 (6)	F(4)–C(15)	1.349 (7)
Rh–C(5)	2.209 (6)	F(5)–C(16)	1.358 (6)
	Bond Angles/deg		
C(1)–C(2)–C(3)	107.9 (5)	C(6)–C(1)–C(2)	123.9 (6)
C(2)–C(3)–C(4)	108.4 (5)	C(7)–C(2)–C(3)	127.8 (5)
C(3)–C(4)–C(5)	107.3 (5)	C(8)–C(3)–C(4)	124.3 (6)
C(4)–C(5)–C(1)	108.2 (5)	C(9)–C(4)–C(5)	125.6 (5)
C(5)–C(1)–C(2)	107.8 (5)	C(10)–C(5)–C(1)	126.3 (5)
P–Rh–Cl	84.58 (7)	C(17)–P–Rh	110.7 (2)
Cl–P–C(11)	92.0 (2)	C(18)–P–Rh	114.0 (2)
P–Rh–C(11)	94.0 (2)	C(19)–P–Rh	121.2 (3)
Rh–C(11)–C(16)	125.6 (4)	C(17)–P–C(18)	102.8 (3)
Rh–C(11)–C(12)	121.0 (4)	C(18)–P–C(19)	104.3 (4)
		C(17)–P–C(19)	101.7 (3)
C(11)–C(12)–C(13)	126.3 (6)	C(11)–C(16)–F(5)	119.9 (5)
C(12)–C(13)–C(14)	118.6 (5)	C(16)–C(15)–F(4)	121.1 (5)
C(13)–C(14)–C(15)	119.4 (5)	C(15)–C(14)–F(3)	120.4 (6)
C(14)–C(15)–C(16)	119.1 (6)	C(14)–C(13)–F(2)	119.4 (5)
C(15)–C(16)–C(11)	125.0 (5)	C(13)–C(12)–F(1)	113.6 (5)

(2) $Cp^*Rh(PMe_3)(C_6F_5)Cl$. The structure of $Cp^*Rh(PMe_3)(C_6F_5)Cl$ was determined in Rochester on an Enraf-Nonius CAD4 diffractometer with graphite-monochromated Mo Kα radiation. An orange-red prism of the compound was mounted with epoxy on a glass fiber. Preliminary cell determination was made with 25 centered reflections with values of χ between 0 and 70°. Routine data collection of one quadrant of data was undertaken on the C-centered monoclinic cell as indicated in Table I. The Molecular Structure Corporation TEXSAN analysis software package was used for data reduction and solution.[25] A Patterson map located the rhodium atom: expansion of the structure with the program DIRDEF revealed non-hydrogen atoms. The molecule was found to sit in a general position in the asymmetric unit. Following isotropic refinement, an absorption correction was applied using the program DIFABS. Full-matrix least-squares anisotropic refinement on the non-hydrogen atoms (with hydrogens attached to carbons in idealized positions) was carried out to convergence. Atomic scattering factors were taken from International Tables.[23] The final refinement of 244 variable parameters converged with $R = 0.036$ and $R_w = 0.045$. Interatomic distances between non-hydrogen atoms and selected bond angles are listed in Table III. Full crystallographic data and a packing diagram are given in the supplementary material (Tables IX–XIII and Figure 6).

Matrix Isolation. The matrix isolation equipment has been described in detail previously.[26] Samples were deposited onto a CsI window cooled by an Air Products CS202 closed-cycle Displex refrigerator to 20 K. BaF_2 windows were used for combined IR and UV/vis experiments. The precursor complexes were sublimed from a right-angled glass tube held at 340 K for $CpRh(PMe_3)(\eta^2\text{-}C_6F_6)$ and 358 K for $Cp^*Rh(PMe_3)(\eta^2\text{-}C_6F_6)$ at the same time as matrix gas (BOC research grade, 99.999%) was deposited through a separate inlet. Deposition lasted for 2–3 h, during which 3.5–6 mmol of matrix gas was deposited. The samples were cooled to 12 K before the IR (Mattson Sirius FTIR spectrometer, with TGS detector and KBr beamsplitter, 1 cm^{-1} resolution, 128 scans coaveraged, 25K data points, 50K transform points) and UV/vis spectra (Perkin-Elmer Lambda 7G spectrometer with Perkin-Elmer data station, 1-nm resolution) were recorded. The sample was irradiated through a quartz window with light from a Philips HPK 125-W mercury arc equipped with a water filter and suitable cutoff filters.

Syntheses. The following were synthesized by literature methods: $CpRh(PMe_3)(C_2H_4)$.[27] $Cp^*Rh(PMe_3)(C_2H_4)$.[28] $Cp^*Rh(PMe_3)(C_6H_5)H$.[29] and $CpIr(PMe_3)H_2$.[30]

Synthesis of $CpRh(PMe_3)(\eta^2\text{-}C_6F_6)$. $CpRh(PMe_3)(C_2H_4)$ (46.5 mg, 0.17 mmol) was placed in an ampule (volume 5 cm^3), and 3 cm^3 of C_6F_6 was added. The yellow solution was photolyzed for 40 h with $\lambda > 285$ nm. The solvent was removed under vacuum to leave an orange solid. The orange solid was sublimed at 75 °C and 4×10^{-4} mbar onto a liquid nitrogen cooled finger: yield = 45.9 mg (62%): NMR data are listed in Table IV; MS m/z (EI, relative intensity) 244 (100) $[M - C_6F_6]^+$. 227 (20). 212 (17). 178 (17). 168 (36) $[CpRh]^+$: IR (KBr disk) ($\bar{\nu}$/cm^{-1} 2000–300 cm^{-1} region) 1695 s. 1616 s. 1499 w. 1442 s. 1409 m. 1348 s. 1337 s. 1308 s. 1286 m. 1260 s. 1228 m. 1108 m. 1093 s. 1038 m. 1011 m. 986 m. 950 s. 927 s. 908 m. 857 m. 833 s. 797 s. 737 m. 689 m. 671 s. 582 s. 482 m. 409 w. 400 w. 395 w. 373 s: UV/vis (C_6H_{12}, λ/nm) 253. 295, 331. 425. Anal. Calcd for $C_{14}H_{14}RhPF_6$: C, 39.37; H, 3.50. Found: C, 39.09; H, 3.28.

Synthesis of $Cp^*Rh(PMe_3)(C_6F_5)Cl$. $Cp^*Rh(PMe_3)(C_2H_4)$ (ca. 50 mg, 0.15 mmol) was placed in an ampule, and 3 cm^3 of C_6F_6 was added. The yellow solution was photolyzed for 40 h. A few drops of $CHCl_3$ were added to the solution. The volatiles were removed under vacuum, and the remaining orange oil was extracted into 0.5 cm^3 of $CHCl_3$ and placed in a small sample tube. A layer of hexane was added slowly on top of the $CHCl_3$ layer, and the solution was left open to air. The product crystallized as small orange crystals suitable for X-ray analysis: NMR data are listed in Table IV; MS (FAB) m/z (relative intensity) 516 (18) $[M]^+$. 481 (100) $[M - Cl]^+$. 313 (17). 243 (72): IR (Nujol mull) ($\bar{\nu}$/cm^{-1} 2000–550 cm^{-1} region) 1497 (w), 1282 (w), 1057 (w). 1027 (w). 953 (m). 863 (w), 676 (w).

Synthesis of $Cp^*Rh(PMe_3)(\eta^2\text{-}C_6F_6)$. C_6F_6 (3 cm^3) was condensed into an ampule containing $Cp^*Rh(PMe_3)(C_6H_5)H$ (ca. 40 mg, 0.1 mmol). The solution was heated to 80 °C for 26 h. The ^1H NMR spectrum after reaction showed greater than 95% conversion to the desired product. The orange compound was sublimed at 80 °C and 1×10^{-3} mbar onto a liquid nitrogen cooled finger: NMR data are listed in Table IV; MS (EI, relative intensity) 500 (0.25) $[M]^+$. 481 (0.9) $[M - F]^+$. 314 (100) $[M - C_6F_6]^+$. 238 (18) $[Cp^*Rh]^+$; IR (Nujol mull $\bar{\nu}$/cm^{-1} 2000–500 cm^{-1} region) 1694 (w). 1615 (w), 1526 (w). 1519 (w). 1497 (w). 1456 (w). 1428 (w). 1418 (w). 1376 (w). 1326 (w). 1303 (w). 1282 (w). 1234 (w), 1075 (w). 1019 (w). 953 (m). 947 (m). 932 (m). 911 (m). 727 (w). 686 (w). 665 (w). 590 (w).

Synthesis of $CpIr(PMe_3)(\eta^2\text{-}C_6F_6)$ and $CpIr(PMe_3)(C_6F_5)H$. C_6F_6 (3 cm^3) was added to a sample of $CpIr(PMe_3)H_2$ (ca. 20 mg, 0.06 mmol). The solution was irradiated for 5 h ($\lambda > 285$ nm). The volatiles were removed under vacuum, and the residue was dissolved in C_6D_6. The ^1H NMR spectrum showed 90% conversion to products: $CpIr(PMe_3)(\eta^2\text{-}C_6F_6)$. 42%; $CpIr(PMe_3)(C_6F_5)H$. 35%; and $CpIr(PMe_3)H_2$. 12%. No attempt was made to purify the products. NMR data are listed in Table IV.

Reaction of $CpRh(PMe_3)(\eta^2\text{-}C_6F_6)$ + $^iPr_3SiH$. Triisopropylsilane (3 cm^3) was added to 25.7 mg (0.06 mmol) of $CpRh(PMe_3)(\eta^2\text{-}C_6F_6)$ in an ampule. The solution was photolyzed with $\lambda > 285$ nm for 45 min. The solvent was removed under vacuum and the residue was dissolved in C_6D_6. NMR data of $CpRh(PMe_3)(Si^iPr_3)H$ in C_6D_6 are as follows: ^1H δ 5.15 (d, J_{PH} = 0.4 Hz, 5 H, C_5H_5). 1.28 (t, J = 7.1 Hz, 18 H, $[(CH_3)_2CH]_3$), 1.10 (sept, J = 7.1 Hz, 3 H, $[(CH_3)_2CH]_3$), 0.97 (dd, J_{PH} = 9.5 Hz, J_{RhH} = 1.1 Hz, 9 H, PMe_3), −14.57 (dd, J_{PH} = 33.4 Hz, J_{RhH} = 30.1 Hz, 1 H, Rh*H*); $^{13}C\{^1H\}$ δ 87.48 (t, $J_{PC} = J_{RhC}$ = 2.2 Hz, C_5H_5). 25.42 (d, J_{PC} = 30.1 Hz, PMe_3). 21.55 (s, $[(CH_3)_2CH]_3$). 19.77 (s, $[(CH_3)_2CH]_3$); $^{31}P\{^1H\}$ δ −0.35 (d, J_{RhP} = 174.1 Hz, PMe_3). Anal. Calcd for $C_{17}H_{36}PRhSi$: C, 50.74; H, 9.02. Found: C, 51.19; H, 9.22.

Reaction of $CpRh(PMe_3)(\eta^2\text{-}C_6F_6)$ with HCl. A solution of $CpRh(PMe_3)(\eta^2\text{-}C_6F_6)$ (ca. 20 mg, 0.05 mmol) in THF (10 cm^3) was stirred in a 50 cm^3 flask under 1 atm of HCl for 1 h. The original orange color darkened to blood red. The product was recrystallized from $CHCl_3$ and identified as $CpRh(PMe_3)Cl_2$ by NMR and mass spectrometry: ^1H NMR ($CpRh(PMe_3)Cl_2$ in $CDCl_3$) δ 5.53 (d, J_{PH} = 1.8 Hz, 5 H, C_5H_5). 1.84 (d, J_{PH} = 12.6 Hz, 9 H, PMe_3); $^{31}P\{^1H\}$ NMR δ 19.20 (d, J_{RhP} =

(24) Motherwell, S.; Clegg, W. *PLUTO, A program for plotting molecular and crystal structures*; University of Cambridge: Cambridge, England, 1978.

(25) (a) $R_1 = \{\sum||F_o| - |F_s||\}/\{\sum|F_o|\}$; $R_2^2 = [\sum w(|F_o| - |F_c|)^2]/[\sum wF_o^2]$, where $w^{-1} = [\sigma^2(F_o) + \rho(F_o^2)^2]^{0.5}$ for the non-Poisson contribution weighting scheme. The quantity minimized was $\sum w(|F_o| - |F_c|)^2$. (b) Molecular Structure Corporation TEXSAN Structure Analysis Package; Molecular Structure Corp.: College Station, TX, 1985.

(26) Haddleton, D. M.; McCamley, A.; Perutz, R. N. *J. Am. Chem. Soc.* **1988**, *110*, 1810.

(27) Werner, H.; Feser, R. *J. Organomet. Chem.* **1982**, *232*, 351.

(28) Klingert, B.; Werner, H. *Chem. Ber.* **1983**, *116*, 1450.

(29) Jones, W. D.; Feher, F. J. *J. Am. Chem. Soc.* **1984**, *106*, 1650.

(30) Heinekey, D. M.; Payne, N. G.; Schulte, G. K. *J. Am. Chem. Soc.* **1988**, *110*, 2303.

Table IV. NMR Data for $(\eta^5\text{-}C_5R_5)M(PMe_3)L$ and $(\eta^5\text{-}C_5R_5)Rh(PMe_3)(X)(Y)$ Complexes in C_6D_6 at 293 K (δ/ppm)

complex	^{1}H Cp/Cp*	^{1}H PMe_3	^{31}P	^{19}F C_6F_6/C_6F_5[a]
$CpRh(PMe_3)(\eta^2\text{-}C_6F_6)$	4.43 (s)	0.83 (dq) (J_{PH} = 10.7, $J_{RhH} = J_{FH}$ = 0.9 Hz)	2.95 (dt) (J_{RhP} = 19.5, J_{FP} = 56 Hz)	−146.7 (m) F^2, $F^{2'}$
				−161.6 (m) F^1, $F^{1'}$ (J_{PF} = 54, J_{RhF} = 15 Hz)
				−173.8 (m) F^3, $F^{3'}$
$Cp^*Rh(PMe_3)(\eta^2\text{-}C_6F_6)$	1.35 (d) (J_{PH} = 2.2 Hz)	1.00 (dq) (J_{PH} = 10.6, $J_{RhH} = J_{FH}$ = 1.2 Hz)	−0.43 (dt) (J_{RhP} = 195, J_{FP} = 67 Hz)	−147.4 (m) F^2, $F^{2'}$
				−158.7 (m) F^1, $F^{1'}$
				−177.5 (m) F^3, $F^{3'}$
$CpIr(PMe_3)(\eta^2\text{-}C_6F_6)$	4.29 (s)	1.01 (dt) (J_{PH} = 10.6, J_{FH} = 0.8 Hz)	−38.63 (t) (J_{FP} = 40.2 Hz)	−147.4 (m) F^2, $F^{2'}$
				−162.5 (m) F^1, $F^{1'}$
				−174.6 (m) F^3, $F^{3'}$
$Cp^*Rh(PMe_3)(C_6F_5)F$	1.10 (d) (J_{PH} = 2.3 Hz)	0.91 (d) (J_{PH} = 11.2 Hz)	6.75 (ddd) (J_{RhP} = 145, J_{FP} = 39, $J_{FP'}$ = 17 Hz)	−114.2 (m) F_{ortho}
				−115.4 (m) F_{ortho}
				−160.3 (t) F_{para}
				−161.6 (m) F_{meta}
				−163.9 (m) F_{meta}
$Cp^*Rh(PMe_3)(C_6F_5)Cl$	1.23 (d) (J_{PH} = 3.4 Hz)	1.12 (dt) (J_{PH} = 10.6, $J_{RhH} = J_{FH}$ = 0.9 Hz)	4.24 (dd) (J_{RhP} = 140, J_{FP} = 22 Hz)	−107.2 (m) F_{ortho}
				−112.9 (m) F_{ortho}
				−161.4 (m) F_{para}
				−162.5 (m) F_{meta}
				−164.7 (m) F_{meta}
$CpIr(PMe_3)(C_6F_5)H$[b]	4.78 (d) (J_{PH} = 0.6 Hz)	0.90 (d) (J_{PH} = 10.8 Hz)	−39.06 (s)	−106.0 (m) F_{ortho}
				−164.0 (t) F_{para}
				−164.7 (m) F_{meta}

[a] The fluorines in the η^2-C_6F_6 complexes are numbered so that F^1 and $F^{1'}$ are bound to the coordinated carbon atoms and F^2 and $F^{2'}$ are ortho to F^1 and $F^{1'}$. [b] The hydride ligand is located at δ −16.19 (dt) (J_{PH} = 34.4, J_{FH} = 3.4 Hz).

123.5 Hz. PMe_3): MS (EI, relative intensity for ^{35}Cl) 314 (12) $[M]^+$, 279 (12) $[M - Cl]^+$, 243 (25) $[CpRh(PMe_3) - H]^+$, 168 (21) $[CpRh]^+$, 111 (100).

Results

Reaction of $CpRh(PMe_3)(C_2H_4)$ with C_6F_6. Photochemical reaction ($\lambda > 285$ nm) of $CpRh(PMe_3)(C_2H_4)$ dissolved in C_6F_6 results in efficient conversion to $CpRh(PMe_3)(\eta^2\text{-}C_6F_6)$, which may be recrystallized from hexane. $CpRh(PMe_3)(\eta^2\text{-}C_6F_6)$ is a moderately air-stable, sublimable complex. It shows a doublet of triplets in the $^{31}P\{^1H\}$ NMR spectrum with a value of J(RhP) of 195 Hz (Table IV), which is typical for a $CpRh^I$ complex.[28] The ^{19}F NMR shows three complex multiplets as would be expected for a rigid structure. Indeed there is no evidence from variable-temperature NMR for any motion of the C_6F_6 ring from −30 (CD_3CN solution) up to 130 °C, at which temperature decomposition sets in (130 °C in $C_6D_5NO_2$). The fluorines bound to the coordinated carbons are identified by their coupling to ^{31}P in a ^{19}F J-resolved spectrum. The ^{1}H NMR spectrum shows the PMe_3 resonance as a doublet of quartets with a large coupling to ^{31}P and the quartet arising from coupling to ^{103}Rh and two equivalent fluorine nuclei. The coupling to fluorine superficially appears to be a five-bond coupling but is probably a consequence of the close contact between the fluorines at the site of η^2-coordination and the phosphine methyl protons (see below). A similar phenomenon is observed in $CpIr(C_2H_4)(\eta^2\text{-}C_6F_6)$.[9] The Cp resonance appears as a singlet at fairly high field (δ 4.43), a chemical shift which proves typical for $CpM(L)(\eta^2\text{-}C_6F_6)$ complexes.

Crystal and Molecular Structure of $CpRh(PMe_3)(\eta^2\text{-}C_6F_6)$. The hexafluorobenzene complex $CpRh(PMe_3)(\eta^2\text{-}C_6F_6)$ crystallizes in space group *Pnma* with a crystallographically imposed mirror plane (Table II and Figure 1a). The C_6F_6 ligand is bonded to the rhodium via two adjacent carbon atoms in a symmetrical arrangement (r(Rh–C(7)) = 2.058 (4) Å). The C_6F_4 unit, C(7)C(8)F(8)C(9)F(9)C(7)′C(8)′F(8)′C(9)′F(9)′, retains its planarity (mean deviation from plane = 0.029 Å), with a maximum deviation of 0.046 Å of one of the fluorine atoms from the best plane (Figure 1b). The dihedral angle between the C_6F_4 plane and the plane formed by RhC(7)C(7)′ is 108.6°. Most conspicuously, the fluorines at the site of η^2-coordination are bent out of the C_6F_4 plane by 43.8° (Figure 1b). The dihedral angle between the normals to the RhC(7)C(7)′ and F(7)C(7)C(7)′F(7)′ planes is 64.8°. The center of the coordinated C–C bond of the C_6F_6 lies 1.935 Å from Rh. The length of the coordinated C–C bond (1.397 (12) Å) is not significantly different from that found in free C_6F_6 (1.394 (7) Å)[31] despite complexation. In contrast, the remaining C–C bond lengths of the C_6F_6 ring are perturbed from the free arene value to form a diene-type configuration, while the uncoordinated diene unit is linked to the coordinated double bond by relatively long C–C bonds (1.473 (8) Å). There is surprisingly little bond length alternation within the uncoordinated diene unit: the difference between C(9)–C(9)′ and C(8)–C(9) is an insignificant 0.023 Å. In the iridium complex $CpIr(C_2H_4)(\eta^2\text{-}C_6F_6)$ the difference is 0.10 (3) Å.[9]

The disorder in the PMe_3 ligand is modeled by allowing for two positions of each methyl group with 50% occupancy in each. In any one molecule, one of the methyl carbons lies very close to a fluorine atom (C···F = 2.773 (17) Å) and another one is also close enough to interact at 3.109 (23) Å. These methyl groups are sufficiently near to the fluorine atoms for the van der Waals radii of hydrogen and fluorine to overlap. The coupling between the methyl protons and ^{19}F in the NMR spectrum implies that this interaction persists in solution.

Reactions of $CpRh(PMe_3)(\eta^2\text{-}C_6F_6)$. Although $CpRh(PMe_3)(\eta^2\text{-}C_6F_6)$ is photostable in C_6F_6, it proves photolabile in other solvents: we have identified its photoproducts from reaction with benzene, PPh_3, Me_3CNC, and $^iPr_3SiH$. We also report its thermal reaction with CO and hydrogen chloride. The photolysis of $CpRh(PMe_3)(\eta^2\text{-}C_6F_6)$ in benzene (4 h, $\lambda > 285$ nm, >95% conversion) cleanly generates the CH insertion product $CpRh(PMe_3)(C_6H_5)H$.[10] In contrast, when a solution of $CpRh(PMe_3)(\eta^2\text{-}C_6F_6)$ in C_6D_6 was heated without UV irradiation at 105 °C for 66 h, the ^{1}H NMR spectrum showed only 6% conversion to $CpRh(PMe_3)(C_6D_5)D$.

The photolysis of $CpRh(PMe_3)(\eta^2\text{-}C_6F_6)$ in C_6D_6 in the presence of PPh_3 leads first to the activation of the solvent to form

(31) Almenningen, A.; Bastiansen, O.; Seip, R.; Seip, H. M. *Acta Chem. Scand.* **1964**, *18*, 2115.

$(\eta^5\text{-}C_5H_5)Rh(PMe_3)(\eta^2\text{-}C_6F_6)$

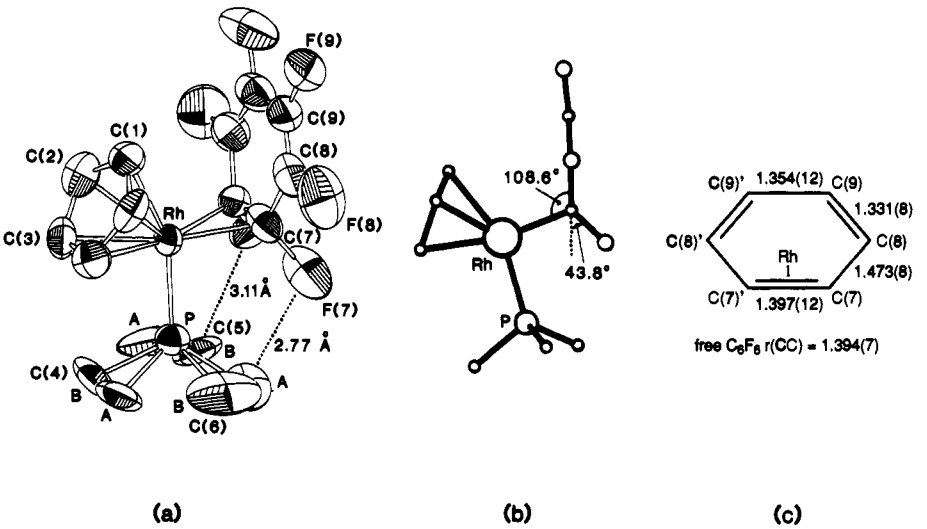

(a) (b) (c)

Figure 1. (a) ORTEP view (ellipsoids at 50% level) of the molecular structure of $CpRh(PMe_3)(\eta^2\text{-}C_6F_6)$. Notice the 2-fold disorder leading to two sets of phosphine methyl groups (A and B). The diagram highlights one short contact and one intermediate contact between these methyl groups and the fluorine atoms. (b) Projection of the structure onto the crystallographic mirror plane showing the planarity of the C_6F_4 moiety of the hexafluorobenzene group and the bending of the remaining two fluorine atoms out of that plane. (c) Diagram showing the bond lengths (angstroms) within the hexafluorobenzene ring illustrating the deviation from a regular hexagon.

$CpRh(PMe_3)(C_6D_5)D$, identified in the $^{31}P\{^1H\}$ NMR spectrum as a doublet of 1:1:1 triplets at δ 13.56. On continued photolysis, the sequential formation of $CpRh(PMe_3)(PPh_3)$[32] and $CpRh(PPh_3)_2$[33] is observed in the $^{31}P\{^1H\}$ NMR spectrum.

An NMR tube containing $CpRh(PMe_3)(\eta^2\text{-}C_6F_6)$ in C_6D_6 with 2 μL of *tert*-butyl isonitrile showed some thermal reaction at room temperature, forming $CpRh(PMe_3)(CNCMe_3)$. On photolysis, stepwise substitution first of the C_6F_6 ligand and then of the PMe_3 ligand leads to the formation of $CpRh(PMe_3)(CNCMe_3)$[34] and $CpRh(CNCMe_3)_2$,[32] respectively.

The photolysis of $CpRh(PMe_3)(\eta^2\text{-}C_6F_6)$ in triisopropylsilane brings about clean conversion to the Si–H activation product $CpRh(PMe_3)(Si^iPr_3)H$. CO displaces the C_6F_6 ligand thermally at room temperature to produce $CpRh(PMe_3)CO$.[35] The thermal reaction of $CpRh(PMe_3)(\eta^2\text{-}C_6F_6)$ with HCl yields the previously unknown $CpRh(PMe_3)Cl_2$ (see the Experimental Section).

In summary, $CpRh(PMe_3)(\eta^2\text{-}C_6F_6)$ is exceptionally photosensitive and both thermal and photochemical reactions of $CpRh(PMe_3)(\eta^2\text{-}C_6F_6)$ are dominated by C_6F_6 loss (Scheme I).

Photochemical Reaction of $Cp^*Rh(PMe_3)(C_2H_4)$ with C_6F_6. The photolysis of a sealed tube containing $Cp^*Rh(PMe_3)(C_2H_4)$ in C_6F_6 for 7 h ($\lambda > 285$ nm) generates one product which appears at δ −0.43 as a doublet of triplets [J(RhP) = 195 Hz] in the $^{31}P\{^1H\}$ spectrum. The conversion was estimated as 25% by integration of the spectrum recorded with inverse gated decoupling. The ^1H, ^{19}F, and ^{31}P NMR data are very similar to those recorded for $CpRh(PMe_3)(\eta^2\text{-}C_6F_6)$ (Table IV). The product is assigned as $Cp^*Rh(PMe_3)(\eta^2\text{-}C_6F_6)$. It may be generated independently by reaction of $Cp^*Rh(PMe_3)(C_6H_5)H$ with C_6F_6 (see below).

Prolonged photolysis (40 h) reduces both the starting material and $Cp^*Rh(PMe_3)(\eta^2\text{-}C_6F_6)$ and generates three additional products A, B, and C. The $^{31}P\{^1H\}$ NMR spectrum now shows three resonances with J(RhP) in the range 140–150 Hz to lower field both of $Cp^*Rh(PMe_3)(C_2H_4)$ and of $Cp^*Rh(PMe_3)(\eta^2\text{-}C_6F_6)$. The product distribution of A:B:C:$Cp^*Rh(PMe_3)(\eta^2\text{-}C_6F_6)$:$Cp^*Rh(PMe_3)(C_2H_4)$ is estimated as 65%:7.8%:9.2%:12.7%:5.6%. The change in chemical shift to lower field and the reduced rhodium–phosphorus coupling constant are both indicative of rhodium(III) species,[28] suggesting that insertion into a C–F bond of C_6F_6 has occurred.

Scheme I. Synthesis and Reactions of $CpRh(PMe_3)(\eta^2\text{-}C_6F_6)$

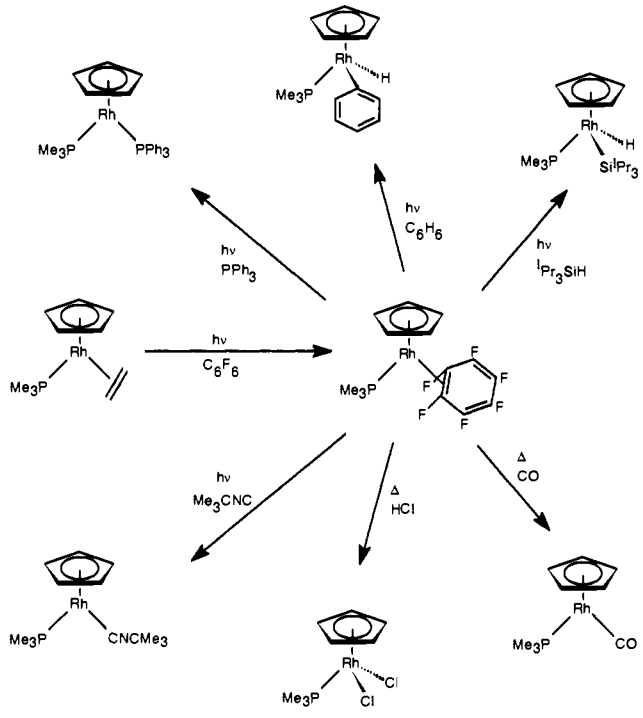

The major new species. A. appears at δ 6.75 as a doublet (J_{RhP} = 145 Hz) of doublet of doublets in the $^{31}P\{^1H\}$ NMR spectrum. The ^1H spectrum shows broad resonances for Cp^* and PMe_3 protons. The ^{19}F NMR spectrum shows five complex resonances of equal area at δ −114.2. −115.4, −160.3, −161.6, and −163.9, assigned as the five fluorine atoms in a coordinated C_6F_5 ring.

(32) Werner, H.; Hofmann, L.; Feser, R.; Paul, W. *J. Organomet. Chem.* **1985**, *281*, 317.
(33) (a) Wakatsuki, Y.; Yamazaki, H. *J. Organomet. Chem.* **1974**, *64*, 393. (b) Belt. S. T.; Duckett, S. B.; Haddleton, D. M.; Perutz, R. N. *Organometallics* **1989**, *8*, 748.
(34) Werner, H.; Lotz, S.; Heiser, B. *J. Organomet. Chem.* **1981**, *209*, 197.
(35) Feser. R.; Werner. H. *J. Organomet. Chem.* **1982**, *233*, 193.

The connectivities of these resonances and those of the Cp*Rh(PMe$_3$)(η^2-C$_6$F$_6$) complex were ascertained from a ^{19}F–^{19}F COSY spectrum. The assignments were also confirmed by comparison with a study made by Bruce on polyfluoroaromatic transition metal complexes.[36] The product B, which appears as a triplet of doublets in the ^{31}P{^{1}H} spectrum, is thought to be CpRh(PMe$_3$)F$_2$ but was not investigated further.[37] A third product, C, formed on prolonged photolysis appears at δ 4.24 as a doublet of doublets in the ^{31}P{^{1}H} spectrum. The ^{1}H NMR spectrum shows a resonance for the Cp* methyl protons and a PMe$_3$ resonance centered at δ 1.12 which appears as a doublet of triplets. The ^{19}F NMR spectrum shows five fluorine resonances of equal area at δ −107.2, −112.9, −161.4, −162.5, and −164.7, which are very similar to those observed for the major rhodium(III) product.

Reaction of these products with CHCl$_3$ simplifies the ^{31}P{^{1}H} NMR spectrum. The starting material Cp*Rh(PMe$_3$)(C$_2$H$_4$) (and probably product B) is converted to Cp*Rh(PMe$_3$)Cl$_2$.[38] The major rhodium(III) product is no longer present in the spectrum. The η^2-C$_6$F$_6$ complex remains, and there is only one other rhodium(III) product which appears as a doublet of doublets. The NMR parameters are extremely similar to those observed for the minor rhodium(III) product, C. The ^{19}F NMR spectrum showed three complex resonances for the η^2-C$_6$F$_6$ complex and five resonances of equal area assigned to the five fluorine atoms in a coordinated C$_6$F$_5$ ring. The product is assigned as Cp*Rh(PMe$_3$)(C$_6$F$_5$)Cl (Table IV). The ^{31}P{^{1}H} NMR spectrum of this product may be explained on the basis that the large doublet splitting is due to rhodium and the smaller one is due to coupling to one ortho fluorine on the C$_6$F$_5$ ring. The ^{19}F NMR spectrum shows that the C$_6$F$_5$ ring is not rotating about the Rh–C bond on the NMR time scale, so that five fluorine resonances are detected. There is no rotation about the Rh–C bond even up to 75 °C, probably due to the steric congestion within the molecule. (In contrast, in the Cp analogue CpRh(PMe$_3$)(C$_6$F$_5$)Br there is a low barrier to internal rotation of the C$_6$F$_5$ group about the Rh–C bond which makes the two ortho and meta positions appear equivalent.)[39,40] The coupling to just one ortho fluorine is also observed in the ^{1}H NMR spectrum for the PMe$_3$ resonance. Small orange crystals were grown from CHCl$_3$/hexane, and X-ray crystallography confirmed the assignment as Cp*Rh(PMe$_3$)(C$_6$F$_5$)Cl.

These observations aid the characterization of the major rhodium(III) product, A, formed on prolonged photolysis of Cp*Rh(PMe$_3$)(C$_2$H$_4$) in C$_6$F$_6$. Compared to the spectrum observed for Cp*Rh(PMe$_3$)(C$_6$F$_5$)Cl, there is just one extra splitting in the ^{31}P{^{1}H} spectrum for A which is created by the phosphorus coupling to a fluorine atom bound directly to rhodium. The major rhodium(III) product is therefore assigned as Cp*Rh(PMe$_3$)(C$_6$F$_5$)F, the product of insertion into a C–F bond of C$_6$F$_6$. The extra coupling to fluorine has the effect of broadening the resonances of Cp*Rh(PMe$_3$)(C$_6$F$_5$)F in the ^{1}H NMR spectrum. The rhodium-bound fluorine ligand has not been located in the ^{19}F NMR spectrum despite much effort, probably because it overlaps with some of the other resonances and would be broadened by coupling to rhodium, phosphorus, and fluorines on the aryl ring. The lack of observation of metal-bound fluorides has been noted previously.[41]

As mentioned above, some Cp*Rh(PMe$_3$)(C$_6$F$_5$)Cl was formed even prior to addition of CHCl$_3$—its proportion increased on heating at the expense of Cp*Rh(PMe$_3$)(C$_6$F$_5$)F. In order to try to eliminate the formation of Cp*Rh(PMe$_3$)(C$_6$F$_5$)Cl on initial photolysis, extra precautions were taken to dry the glassware, and the C$_6$F$_6$ (nominally 99.9%) was distilled and dried over CaH$_2$ or molecular sieves. However, the formation of Cp*Rh(PMe$_3$)(C$_6$F$_5$)Cl was still observed (Cp*Rh(PMe$_3$)(C$_6$F$_5$)F:Cp*Rh(PMe$_3$)(C$_6$F$_5$)Cl = 3:1 after 53 h of photolysis), probably because of traces of chlorofluorobenzenes in the C$_6$F$_6$. GC/MS of the C$_6$F$_6$ revealed that the principal impurity was C$_6$F$_5$Cl. Other impurities were at least 400 times less abundant. To test the hypothesis that Cp*Rh(PMe$_3$)(C$_6$F$_5$)Cl derived from C$_6$F$_5$Cl impurities, the reaction was repeated with C$_6$F$_6$ which had been doped with 1% C$_6$F$_5$Cl. The ^{31}P{^{1}H} NMR spectrum did not show the presence of any Cp*Rh(PMe$_3$)(C$_6$F$_5$)F. The major product formed was Cp*Rh(PMe$_3$)Cl$_2$, which probably derived from chlorination of Cp*Rh(PMe$_3$)(C$_2$H$_4$). The presence of some Cp*Rh(PMe$_3$)(C$_6$F$_5$)Cl is shown both by NMR and by mass spectrometry (m/z 516 [M]$^+$). We conclude that Cp*Rh(PMe$_3$)(C$_6$F$_5$)Cl is formed by reaction of Cp*Rh(PMe$_3$)(C$_6$F$_5$)F with C$_6$F$_5$Cl impurity.

The observation of sequential growth of Cp*Rh(PMe$_3$)(η^2-C$_6$F$_6$) and Cp*Rh(PMe$_3$)(C$_6$F$_5$)F suggests that the C–F insertion product could be formed from the η^2-C$_6$F$_6$ product. Accordingly, a sample of Cp*Rh(PMe$_3$)(η^2-C$_6$F$_6$) was isolated by sublimation and redissolved in C$_6$F$_6$. After photolysis (3 h, $\lambda > 285$ nm) the ^{31}P{^{1}H} NMR spectrum showed partial conversion to the C–F activation products (Rh(C$_6$F$_5$)F:Rh(C$_6$F$_5$)Cl:Rh(η^2-C$_6$F$_6$) = 43%:38%:19%). We attempted to convert Cp*Rh(PMe$_3$)(η^2-C$_6$F$_6$) to Cp*Rh(PMe$_3$)(C$_6$F$_5$)F in the absence of excess C$_6$F$_6$. However, photolysis in benzene-d_6 only effected intermolecular benzene activation to form Cp*Rh(PMe$_3$)(C$_6$D$_5$)D.

Thermal Reaction of Cp*Rh(PMe$_3$)(C$_6$H$_5$)H with C$_6$F$_6$. The complex Cp*Rh(PMe$_3$)(C$_6$H$_5$)H has been shown to be a good thermal source of [Cp*Rh(PMe$_3$)].[29] Accordingly, a sample of Cp*Rh(PMe$_3$)(C$_6$H$_5$)H was heated in C$_6$F$_6$ for 27 h at 80 °C, resulting in the elimination of benzene and the formation of Cp*Rh(PMe$_3$)(η^2-C$_6$F$_6$). However, even when the temperature was raised to 110 °C for 30 h, there was no evidence in the NMR spectra for any products formed from insertion into a C–F bond of C$_6$F$_6$. Thus the C–F insertion step has only been achieved photochemically. Due to the inability to interconvert Cp*Rh(PMe$_3$)(η^2-C$_6$F$_6$) and Cp*Rh(PMe$_3$)(C$_6$F$_5$)F thermally, the relative stabilities of these two species remain unknown. The reactions of Cp*Rh(PMe$_3$)(C$_2$H$_4$) and Cp*Rh(PMe$_3$)(C$_6$H$_5$)H with C$_6$F$_6$ are summarized in Scheme II.

Scheme II. Photochemical Reactions of Cp*Rh(PMe$_3$)(C$_2$H$_4$) and Thermal Reaction of Cp*Rh(PMe$_3$)(Ph)H with Hexafluorobenzene

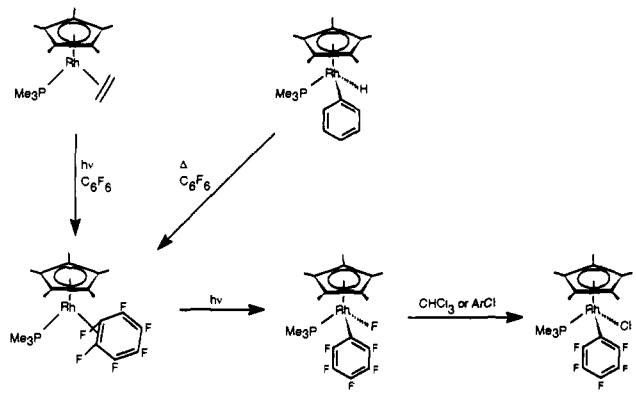

The Crystal and Molecular Structure of Cp*Rh(PMe$_3$)(C$_6$F$_5$)Cl. The complex Cp*Rh(PMe$_3$)(C$_6$F$_5$)Cl crystallizes in space group $C2/c$. The structure shows the distances and angles to be quite normal for a molecule of this type (Figure 2 and Table III). The Rh–C(11) bond distance of 2.070 (5) Å is virtually identical to that observed for Cp*Rh(PMe$_3$)(C$_6$H$_5$)Br.[40] The C–C bond lengths of the C$_6$F$_5$ ring are very uniform. The Rh–C$_6$F$_5$ bond lies at an angle of 12° to the C$_6$F$_5$ plane, with the result that the perpendicular distance from the rhodium atom to the plane is 0.409 Å. The dihedral angle between the C$_6$F$_5$ plane and the C$_5$Me$_5$

(36) Bruce, M. I. *J. Chem. Soc. A* **1968**, 1459.
(37) Product B (Cp*Rh(PMe$_3$)F$_2$) is generated in higher yield by photolysis of Cp*Rh(PMe$_3$)H$_2$ in C$_6$F$_6$ (^{31}P NMR in C$_6$D$_6$ δ 12.0 (dt, J_{RhP} = 144 Hz, J_{PF} = 10 Hz)).
(38) Isobe, K.; Bailey, P. M.; Maitlis, P. M. *J. Chem. Soc., Dalton Trans.* **1981**, 2003.
(39) (a) The barrier to internal rotation of the C$_6$F$_5$ group of CpRh(PMe$_3$)(C$_6$F$_5$)Br is $\Delta G^{\ddagger}$ = 39 ± 2 kJ mol^{-1}. (b) Partridge, M. G. D.Phil. Thesis, University of York, U.K., 1992.
(40) The barrier to internal rotation of the phenyl group of Cp*Rh(PMe$_3$)(Ph)Br is 58.5 kJ mol^{-1}: Jones, W. D.; Feher, F. J. *Inorg. Chem.* **1984**, *23*, 2376.
(41) Doherty, N. M.; Hoffman, N. W. *Chem. Rev.* **1991**, *91*, 553.

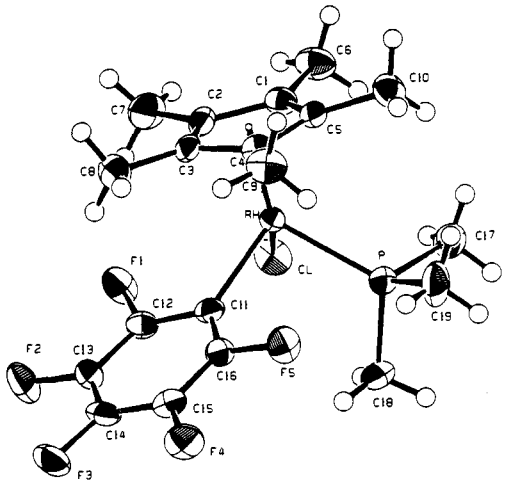

Figure 2. ORTEP view of the molecular structure of Cp*Rh-(PMe_3)(C_6F_5)Cl. Ellipsoids are shown at the 50% level.

plane is 20.4°. The structure shows that the plane of the C_6F_5 ring is oriented so as to minimize steric hindrance with the C_5Me_5 ring. The phosphine methyl groups are staggered with respect to the C_5Me_5 ring and the C_6F_5 ring to reduce steric hindrance. A space-filling representation shows that the Cp* methyl groups obstruct any rotation of the C_6F_5 group.

Photochemical Reaction of CpIr(PMe_3)H_2 with C_6F_6. Irradiation of CpIr(PMe_3)H_2 in C_6F_6 (5 h with $\lambda > 285$ nm) effected 87% conversion to two principal products present in a 6:5 ratio. The NMR data of the major product are remarkably similar to those observed for CpRh(PMe_3)(η^2-C_6F_6), the only difference being the lack of a coupling to rhodium (Table IV). The major product is therefore assigned as CpIr(PMe_3)(η^2-C_6F_6). The second product has a Cp resonance at δ 4.78 and a PMe_3 resonance at δ 0.90 in the ^1H spectrum. In the high-field region of the spectrum, there is a hydride resonance at δ −16.19 which appears as a doublet of triplets. The ^{19}F NMR spectrum shows three resonances at δ −106.0, −164.0, and −164.7 in the ratio 2:1:2. The chemical shifts of these three resonances are very similar to those observed for CpRh(PMe_3)(C_6F_5)H.[42] The $^{31}P\{^1H\}$ spectrum shows a singlet at δ −39.06. The complex is assigned as CpIr(PMe_3)(C_6F_5)H. The extra splittings in the hydride resonance appear to result from coupling to the two equivalent ortho fluorines. The equivalence of the ortho fluorines in this complex implies that rotation about the Ir–C bond is rapid on the NMR time scale.

Photochemical Reaction of CpIr(PMe_3)D_2 with C_6F_6. In order to identify the hydride source, a sample of CpIr(PMe_3)$D_{2-x}H_x$ (x = 0–2, overall 70% deuterated) was photolyzed in C_6F_6 for 15 min. The ^1H NMR spectrum (recorded in C_6F_6) showed that both CpIr(PMe_3)(η^2-C_6F_6) and CpIr(PMe_3)(C_6F_5)$D_{1-y}H_y$ (y = 0–2) were already present although there was only ca. 15% conversion to products. The conversion increased to 32% after an additional 30 min of photolysis and 60% after a total of 105 min of irradiation, but the ratio of the two products remained unchanged giving a final distribution of CpIr(PMe_3)(η^2-C_6F_6):CpIr(PMe_3)(C_6F_5)$D_{1-y}H_y$:CpIr(PMe_3)$D_{2-x}H_x$ = 1:2:2. The iridium hydride region of the spectrum shows there to be two hydride resonances in the ratio 2:1 [CpIr(PMe_3)($D_{2-x}H_x$:CpIr(PMe_3)(C_6F_5)$D_{1-y}H_y$]. This observation shows that there is quantitative transfer of the hydride from the starting material to the product, suggesting an intramolecular mechanism. Further confirmation came from the $^2H\{^1H\}$ NMR spectrum, which showed two deuteride resonances in the ratio 2:1 [CpIr(PMe_3)D_xH_{2-x}:CpIr(PMe_3)(C_6F_5)$D_{1-y}H_y$]. The demonstration that both the η^2-C_6F_6 complex and the C–F insertion product are observed to form concurrently suggests that the two products are formed by two distinct parallel pathways (Scheme III).

Scheme III. Photochemical Reactions of CpIr(PMe_3)H_2 with Hexafluorobenzene

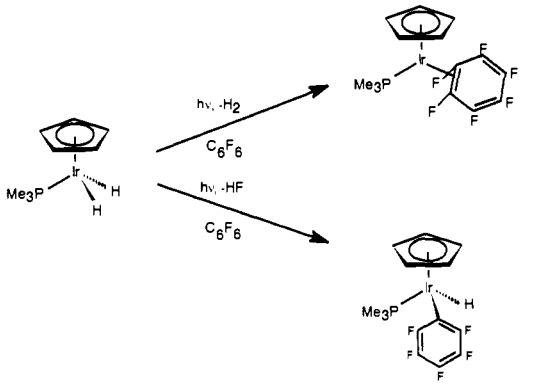

Table V. IR Data ($\bar{\nu}$/cm^{-1}) of CpRh(PMe_3)(η^2-C_6F_6) (3000–900 cm^{-1}) and Cp*Rh(PMe_3)(η^2-C_6F_6) (3000–500 cm^{-1}) in Argon Matrices at 12 K

CpRh(PMe_3)(η^2-C_6F_6)	Cp*Rh(PMe_3)(η^2-C_6F_6)	assignment	
2986. 2977 (w)	2987. 2967 (w)	$\nu(CH_3)_{sym}$	PMe_3
2933. 2923 (w)		ν(CH)	Cp
2913 (w)	2914 (w)	$\nu(CH_3)_{asym}$	PMe_3
1701. 1697 (w)	1699 (w)	ν(C=C)	C_6F_6
1619 (w)	1621 (w)	ν(C=C)	C_6F_6
	1605 (w)		
	1504 (w)		
1444 (w)	1439 (w)		C_6F_6
1427. 1422 (w)	1427. 1423 (w)	$\delta(CH_3)_{asym}$	PMe_3
1371 (w)	1383 (w)		C_6F_6
1356 (w)			C_6F_6
1341 (w)	1343 (w)		C_6F_6
1317 (w)	1315 (w)		C_6F_6
1307 (w)	1306 (w)	$\delta(CH_3)_{sym}$	PMe_3
1289. 1286 (w)	1286. 1283 (w)	$\delta(CH_3)_{asym}$	PMe_3
1276 (w)	1257 (w)	ν(CF)	C_6F_6
1098 (w)	1096 (w)	δ(CH)	Cp
	1091 (w)		
958 (s)	958. 954 (w)	ρ(CH)	PMe_3
948 (w)	946. 942 (w)	ρ(CH)	PMe_3
937 (m)	928 (m)	ρ(CH)	PMe_3
	688 (w)		
	673 (w)		
	596 (w)		

Photochemistry in Matrices: (a) CpRh(PMe_3)(η^2-C_6F_6) in Solid Argon. Our success in studying CpRh(PMe_3)(C_2H_4) by matrix isolation[43] prompted us to examine the photochemistry of (η^5-C_5R_5)Rh(PMe_3)(η^2-C_6F_6) (R = H, Me) in low-temperature matrices. The IR spectrum of CpRh(PMe_3)(η^2-C_6F_6) isolated in high dilution in an argon matrix at 12 K (Figure 3a) shows bands at 1427, 1289, and 958 cm^{-1}, characteristic of the PMe_3 ligand, and at 1701, 1619, 1444, and 1356 cm^{-1}, characteristic of the coordinated C_6F_6 ligand (Table V). The UV/vis spectrum shows shoulders at 291 and 333 nm. Irradiation for 15 min with $\lambda > 210$ nm depletes the bands of the starting material by 17% and results in the formation of several bands, including those at 1533. 1506, 1018, and 997 cm^{-1}. On further photolysis with $\lambda > 210$ nm, the yield of these bands increases and depletion of the bands of CpRh(PMe_3)(η^2-C_6F_6) reaches a total of 31% (Figure 3b). No bands are observed in the ν(RhH) region, 2100–2000 cm^{-1}. The UV/vis spectrum after photolysis shows the presence of a band at ca. 490 nm.

When hexafluorobenzene was isolated in an argon matrix directly in a separate experiment, three intense bands were detected at 1531 (ν(C=C)), 1018, and 999 cm^{-1} (ν(CF)) in the IR spectrum. We are therefore able to assign the intense bands at

(42) CpRh(PMe_3)(C_6F_5)H was synthesized by photolysis of CpRh(PMe_3)(C_2H_4) in C_6F_5H: Partridge, M. G. D.Phil. Thesis, University of York, York, U.K., 1992. Reaction with other partially fluorinated arenes also resulted in CH oxidative addition.

(43) Bell, T. W.; Haddleton, D. M.; McCamley, A.; Partridge, M. G.; Perutz, R. N.; Willner, H. *J. Am. Chem. Soc.* **1990**, *112*, 9212.

Table VI. IR Data ($\bar{\nu}$/cm^{-1}) for X ($CpRh(PMe_3)(C_6F_5)F$) and X* ($Cp^*Rh(PMe_3)(C_6F_5)F$) in Ar Matrices at 12 K Compared with Data for $CpRh(PMe_3)(C_6F_5)Br$ and $Cp^*Rh(PMe_3)(C_6F_5)Cl$ in Nujol Mulls at 300 K

X = $CpRh(PMe_3)(C_6F_5)F$		$CpRh(PMe_3)(C_6F_5)Br$
argon	nitrogen	Nujol
1506 (m)	1506 (m)	1501 (m)
1460 (w)	1461 (w)	*a*
1456 (w)	1455 (w)	*a*
1068 (w)	1068 (w)	1064 (w)
1060 (w)	1059 (w)	1054 (w)
X* = $Cp^*Rh(PMe_3)(C_6F_5)F$ argon		$Cp^*Rh(PMe_3)(C_6F_5)Cl$ Nujol
1502 (m)		1497 (m)
1454 (w)		*a*
1272 (w)		1282 (w)
1063 (w)		
1058 (w)		1058 (w)
1030 (w)		
960 (s)		954 (s)
775 (w)		

[a] Bands are masked by Nujol peaks.

1533, 1018, and 997 cm^{-1}, which appear on photolysis of $CpRh(PMe_3)(\eta^2\text{-}C_6F_6)$, to expelled C_6F_6. The "free" C_6F_6 experiences negligible perturbation by the remaining organometallic. The dissociation of C_6F_6 would leave a $CpRh(PMe_3)$ fragment. The absence of bands in the ν(RhH) region also rules out the product formed by cyclometalation of the PMe_3 ligand.[44] Further evidence for the assignment to the 16-electron fragment, $CpRh(PMe_3)$, comes from the matrix photochemistry of $CpRh(PMe_3)H_2$ which will be reported elsewhere.[39b]

In addition to release of C_6F_6, the photolysis of $CpRh(PMe_3)(\eta^2\text{-}C_6F_6)$ in an argon matrix generates a second product, X, with an IR band at 1506 cm^{-1} and others elsewhere in the region characteristic of fluoroarenes (Figure 3b and Table VI). The identity of product X will be discussed below.

(b) $Cp^*Rh(PMe_3)(\eta^2\text{-}C_6F_6)$ in an Argon Matrix. The IR spectrum of $Cp^*Rh(PMe_3)(\eta^2\text{-}C_6F_6)$ isolated in high dilution in an argon matrix at 12 K is very similar to that of the Cp analogue (Table V). Irradiation for 10 min with $\lambda > 210$ nm brings about a 23% depletion in bands of the starting material. The main product bands are at 1531, 1502, 1454, 1063, 1058, 996, and 959 cm^{-1}. Further photolysis (total of 2.5 h) with $\lambda > 210$ nm increases the yield of these bands and depletes those of the starting material by an additional 40% (Figure 3c). The bands at 1531 and 996 cm^{-1} can be assigned to expelled C_6F_6, while the remainder are assigned to product X* because of their similarity to X observed in the $CpRh(PMe_3)(\eta^2\text{-}C_6F_6)$/Ar experiment. The absorbance ratio of expelled C_6F_6 to X in the Cp case is about 2:1 (comparison of the bands at 1530 and 1506 cm^{-1}). The same comparison for the Cp* experiment reveals a ratio of about 1:4 (compare Figure 3b,c). The IR data for X* are listed in Table VI.

(c) $CpRh(PMe_3)(\eta^2\text{-}C_6F_6)$ in a 2%CO/Argon Matrix. Irradiation of $CpRh(PMe_3)(\eta^2\text{-}C_6F_6)$ isolated in an argon matrix doped with 2% CO for 1 min with $\lambda > 285$ nm generates intense bands at 1945, 1533, 1018, and 997 cm^{-1} and depletes the bands of the starting material by 25%. The band at 1945 cm^{-1} is assigned as the ν(CO) band of $CpRh(PMe_3)CO$, which has previously been studied in matrices.[43] The remaining three new bands produced on photolysis are assigned to expelled C_6F_6. An additional 5 min of photolysis with $\lambda > 285$ nm increases the intensity of the bands at 1945, 1533, 1018, and 997 cm^{-1} and causes a total of 65% depletion of the starting material bands. There are no bands present for the product X as observed in experiments with pure argon as the matrix host. On further photolysis two new bands are observed at 2048 and 1984 cm^{-1} which are assigned to the ν(CO) bands of $CpRh(CO)_2$.[45] Prolonged irradiation increases

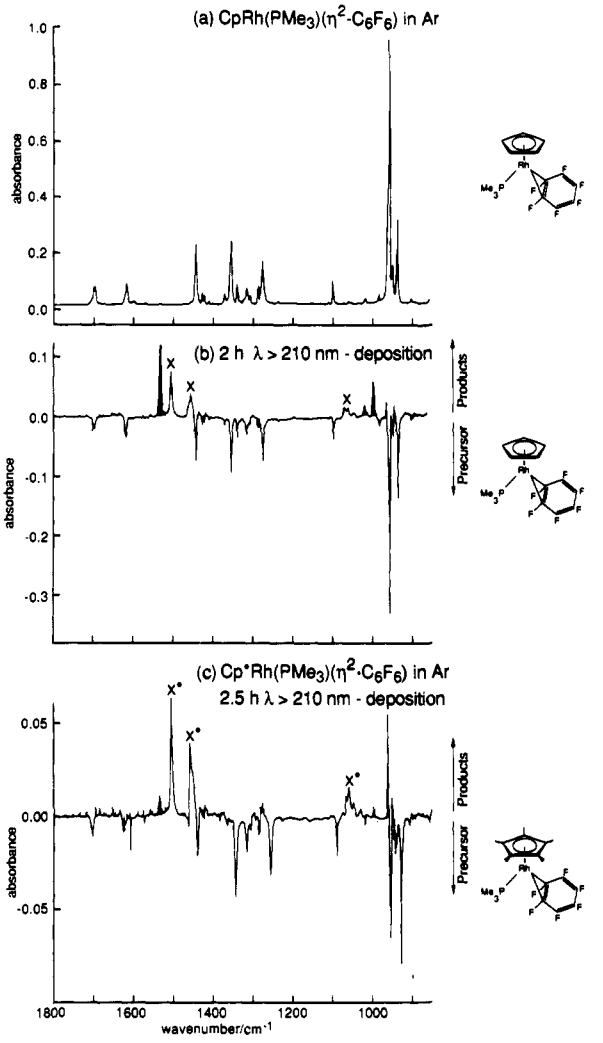

Figure 3. (a) IR spectrum in the region 900–1800 cm^{-1} of $CpRh(PMe_3)(\eta^2\text{-}C_6F_6)$ isolated in an argon matrix at 12 K (135-min deposition, 3.8 mmol of argon deposited, sublimation temperature 67 °C). (b) Difference spectrum relative to spectrum a recorded following 2 h of UV irradiation ($\lambda > 210$ nm), showing loss of precursor and gain of X and C_6F_6 (filled in black). (c) Difference spectrum from an analogous experiment with $Cp^*Rh(PMe_3)(\eta^2\text{-}C_6F_6)$ (210-min deposition, 6.3 mmol of argon deposited, sublimation temperature 85 °C) showing formation of X* and traces of C_6F_6 (black).

the yield of these products at the expense of the bands of $CpRh(PMe_3)(\eta^2\text{-}C_6F_6)$ (Figure 4a).

(d) $CpRh(PMe_3)(\eta^2\text{-}C_6F_6)$ in a Nitrogen Matrix. Irradiation of $CpRh(PMe_3)(\eta^2\text{-}C_6F_6)$ isolated in a nitrogen matrix for 10 min with $\lambda > 285$ nm releases C_6F_6 into the matrix (bands at 1534, 1018, and 997 cm^{-1}) and generates some product X with bands at 1506, 1461, 1455, 1068, and 1059 cm^{-1}. In addition, a group of bands is formed at 2122–2108 cm^{-1}, with the most intense at 2108 cm^{-1}. After further irradiation with $\lambda > 285$ nm (150 min) followed by $\lambda > 210$ nm (110 min), the yield of the bands at 2122 and 2118 cm^{-1} increases relative to the band at 2108 cm^{-1}, and a substantial increase is observed in the intensities of the bands of X (Figure 4b). The product with bands at ca. 2100 cm^{-1} is assigned as $CpRh(PMe_3)N_2$ by comparison with the matrix photolysis of $CpRh(PMe_3)(C_2H_4)$ in nitrogen matrix.[43] A single band at 2118 cm^{-1} is observed on photolysis of $CpRh(PMe_3)(C_2H_4)$, whereas several bands are detected in the ν(NN) region following photolysis of $CpRh(PMe_3)(\eta^2\text{-}C_6F_6)$, probably because $CpRh(PMe_3)N_2$ is present in different orientations relative to the C_6F_6.[46]

(44) See, for example: Chiu, K. W.; Wong, W. K.; Wilkinson, G. *J. Chem. Soc., Chem. Commun.* **1981**, 4551.

(45) Rest, A. J.; Whitwell, I.; Graham, W. A. G.; Hoyano, J. K.; McMaster, A. D. *J. Chem. Soc., Dalton Trans.* **1987**, 1181.

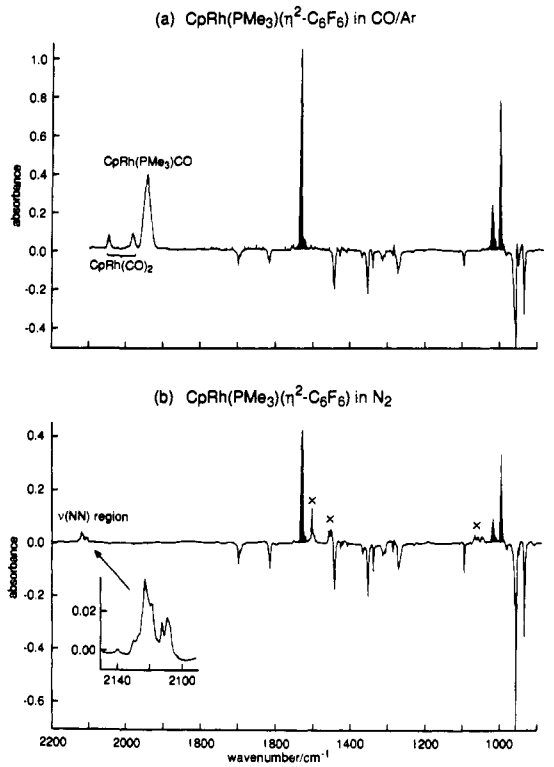

Figure 4. IR difference spectrum relative to the deposition spectrum following 71 min of photolysis ($\lambda > 285$ nm) of $CpRh(PMe_3)(\eta^2\text{-}C_6F_6)$ isolated in a CO/Ar (2:98) matrix. Note the release of C_6F_6 (shaded black) and carbonyl products but absence of X. (b) IR difference spectrum relative to deposition spectrum after 160 min of irradiation with $\lambda > 285$ nm followed by 110 min of photolysis with $\lambda > 210$ nm of $CpRh(PMe_3)(\eta^2\text{-}C_6F_6)$ in a dinitrogen matrix. Note the release of C_6F_6, formation of X, and formation of bands in the NN stretching region (see expansion).

The Identity of Products X and X*. The photolysis of $CpRh(PMe_3)(\eta^2\text{-}C_6F_6)$ in an argon matrix expels some C_6F_6 and also generates a second product X, the major bands of which are at 1506, 1456, 1068, and 1060 cm^{-1}. Similarly, the products of irradiation of $CpRh(PMe_3)(\eta^2\text{-}C_6F_6)$ in a nitrogen matrix are C_6F_6, $CpRh(PMe_3)N_2$, and product X. The photolysis in an argon matrix doped with 2% CO yields only $CpRh(PMe_3)CO$ and C_6F_6.

The irradiation of $Cp^*Rh(PMe_3)(\eta^2\text{-}C_6F_6)$ in an argon matrix generates a small amount of C_6F_6. The major product, X*, has bands at 1502, 1454, 1063, and 1058 cm^{-1}.

We showed above that the photolysis of $Cp^*Rh(PMe_3)(C_2H_4)$ dissolved in liquid C_6F_6 initially yields the $\eta^2\text{-}C_6F_6$ complex, which on further photolysis generates the C–F activation product $Cp^*Rh(PMe_3)(C_6F_5)F$. The photolysis of $CpRh(PMe_3)(C_2H_4)$ in C_6F_6 only produces $CpRh(PMe_3)(\eta^2\text{-}C_6F_6)$ under the conditions of the experiment.

The IR spectrum of $Cp^*Rh(PMe_3)(C_6F_5)Cl$ in a Nujol mull shows bands at 1497, 1058, and 954 cm^{-1} (Table VI), within 5 cm^{-1} of those observed for X* generated on photolysis of $Cp^*Rh(PMe_3)(\eta^2\text{-}C_6F_6)$ in argon matrices. The IR spectrum of $CpRh(PMe_3)(C_6F_5)Br$ in a Nujol mull shows bands at 1501, 1064, and 1054 cm^{-1}, within 5 cm^{-1} of those of X. The IR data in Nujol mulls provide excellent evidence that X and X* are the C–F insertion products $(\eta^5\text{-}C_5R_5)Rh(PMe_3)(C_6F_5)F$ (R = H or Me) formed on photolysis of $(\eta^5\text{-}C_5R_5)Rh(PMe_3)(\eta^2\text{-}C_6F_6)$ in matrices. Further support for this conclusion is reached by comparison with a series of $CpRh(L)(C_6F_5)Cl$ complexes which show very similar bands to products X and X*.[47] We can also exclude the possibility

(46) The C_6F_6 ligand may move further away from the $CpRh(PMe_3)$ fragment on prolonged photolysis causing alteration of the spectrum. A similar phenomenon has been observed with $Fe(CO)_4$ and CO: Poliakoff, M.; Turner, J. J. *J. Chem. Soc., Dalton Trans.* **1973**, 1351.

(47) Mukhedkar, A. J.; Mukhedkar, V. A.; Green, M.; Stone, F. G. A. *J. Chem. Soc. A* **1970**, 3158.

Scheme IV. Matrix Photochemistry of $CpRh(PMe_3)(\eta^2\text{-}C_6F_6)$ and $Cp^*Rh(PMe_3)(\eta^2\text{-}C_6F_6)$

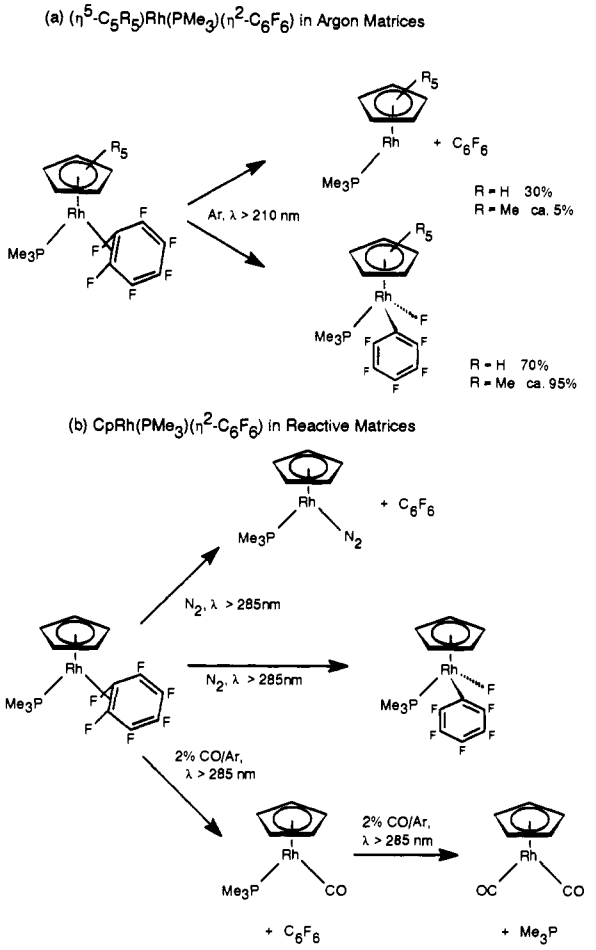

that X is an $\eta^4\text{-}C_6F_6$ complex since the bands observed in the IR spectrum of $Cp^*Ir(\eta^4\text{-}C_6F_6)$ do not resemble those of product X.[9] Since C_6F_6 loss is the only photoprocess observed in CO/Ar matrices, we may use the difference spectra to calculate the relative band areas of the C_6F_6 band at 1533 cm^{-1} and the $CpRh(PMe_3)(\eta^2\text{-}C_6F_6)$ band at 1444 cm^{-1} (ca. 4.4:1). By comparison of the areas of the corresponding bands in other matrices, we can deduce that C_6F_6 loss accounts for ca. 30 ± 5% of the reaction in pure argon and 60 ± 5% in the nitrogen matrix. If we assume equal extinction coefficients for the C_6F_5 ν(CC) vibration of the Cp and Cp* complexes, there is only a ca. 5 ± 2% C_6F_6 loss in the Cp* case. In each case, C–F insertion accounts for the remainder. The photochemistry of $CpRh(PMe_3)(\eta^2\text{-}C_6F_6)$ in matrices is summarized in Scheme IV.

Discussion

In this article, we have reported the characterization of three $\eta^2\text{-}C_6F_6$ complexes: $CpRh(PMe_3)(\eta^2\text{-}C_6F_6)$, $Cp^*Rh(PMe_3)(\eta^2\text{-}C_6F_6)$, and $CpIr(PMe_3)(\eta^2\text{-}C_6F_6)$. Far from being an inert solvent as was suggested for a very similar system,[48] C_6F_6 is highly reactive and proves to be a useful and effective ligand capable of yielding stable complexes coordinated through two or four carbons.[49] Although these complexes have a d^8 configuration and the $CpM(PMe_3)$ are fragments highly susceptible to oxidative addition with other arenes and with trialkylsilanes, hexafluoro-

(48) Marx, D. E.; Lees, A. J. *Inorg. Chem.* **1988**, *27*, 1121.

(49) As yet, the published evidence for coordination of C_6F_6 through all six carbon atoms is confined to products of metal vapor synthesis of the type $Cr(\eta^6\text{-arene})(\eta^6\text{-}C_6F_6)$: Middleton, R.; Hull, J. R.; Simpson, S. R.; Tomkinson, C. H.; Timms, P. L. *J. Chem. Soc., Dalton Trans.* **1973**, 120. Kahn, S. D.; Hehre, W. J.; Bartmess, J. E.; Caldwell, G. *Organometallics* **1984**, *3*, 1740. McGlinchey, M. J.; Tan, T. S. *J. Am. Chem. Soc.* **1976**, *98*, 2271. We have also synthesized $[CpIr(\eta^6\text{-}C_6F_6)](PF_6)_2$; see: Partridge, M. G. D.Phil. Thesis, University of York, York, U.K., 1992.

benzene is able to arrest the oxidative addition process. as explained in the Introduction. The ability of C_6F_6 to act as a donor may be estimated from its ionization energy of 10.2 eV, which is 0.9 eV greater than that of benzene but still 0.3 eV less than that of ethene.[50] The electron affinity has been variously measured as 0.52 or 0.86 eV compared with −1.15 eV for benzene,[51] demonstrating the power of C_6F_6 as an electron acceptor. The HOMO of C_6F_6 is the $e_{1g}(\pi)$ orbital as for benzene. However, the nature of the LUMO is less certain because of ambiguities in the structure of $[C_6F_6]^{\bullet-}$.[52] The most satisfying account suggests that the $e_{2u}(\pi^*)$ and $e_{2u}(CF\ \sigma^*)$ orbitals mix via the second-order Jahn–Teller effect, resulting in a symmetric out-of-plane displacement of pairs of C–F bonds.[53] The anion radical would then occupy a $^2A_2$ state in C_{2v} symmetry. Such mixing of σ^* character into the LUMO has relevance both to the coordination of hexafluorobenzene and to C–F bond cleavage.

The most striking aspect of the structure of $CpRh(PMe_3)(\eta^2\text{-}C_6F_6)$, like that of $CpIr(C_2H_4)(\eta^2\text{-}C_6F_6)$,[9] lies in the distortion of the hexafluorobenzene. Two C–F bonds are bent by 43.8° from the plane of the remainder of the ligand, which adopts a coordinated ene–diene distortion. Unlike the iridium complex, there is no lengthening of the coordinated double bond.

As yet, we have no evidence that $CpRh(PMe_3)(\eta^2\text{-}C_6F_6)$ undergoes C–F insertion *in solution*. In contrast, both $Cp^*Rh(PMe_3)(C_2H_4)$ and $CpIr(PMe_3)H_2$ react with hexafluorobenzene to form (pentafluorophenyl)metal products. That these compounds undergo C–F insertion by different routes is highlighted by the nature of the products and their pattern of growth.

The rhodium system gives rise to the fluoro complex $Cp^*Rh(PMe_3)(C_6F_5)F$ via the $\eta^2\text{-}C_6F_6$ complex. The reaction is demonstrated to be a photochemical analogue of the Parshall mechanism for benzene activation (eqs 3 and 4) by the arguments below.[54]

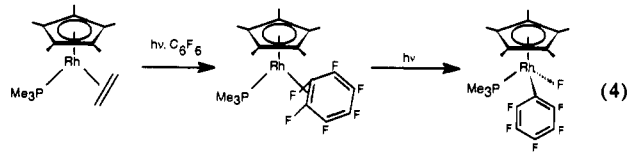

(4)

The C–F insertion product is formed only on prolonged photolysis of the ethene complex, whereas the $\eta^2\text{-}C_6F_6$ product is formed immediately and decays on prolonged photolysis. C–F insertion is also observed on irradiation of a pure sample of the $\eta^2\text{-}C_6F_6$ complex in C_6F_6. This reaction proves that $Cp^*Rh(PMe_3)(\eta^2\text{-}C_6F_6)$ is an effective source for C–F activation, but does not prove intramolecularity since C_6F_6 is used as the solvent. Attempts to replace the C_6F_6 solvent by benzene failed. because then only loss of C_6F_6 was observed. However, further evidence for intramolecularity comes from the observation that $Cp^*Rh(PMe_3)(\eta^2\text{-}C_6F_6)$ undergoes insertion to form $Cp^*Rh(PMe_3)(C_6F_5)F$ on irradiation in an argon matrix at 12 K. This reaction must involve the same C_6F_6 molecule as was coordinated before photolysis.

There is one more link in the chain of evidence for the η^2-arene route to C–F insertion (eq 4). If the photoprocess simply expelled C_6F_6 from $Cp^*Rh(PMe_3)(\eta^2\text{-}C_6F_6)$, we should have been able to induce C–F activation with a thermal source of $Cp^*Rh(PMe_3)$. The thermal reaction would then have yielded $Cp^*Rh(PMe_3)(C_6F_5)F$ or the corresponding chloride formed by scavenging chlorinated impurities, yet neither was observed. Instead we generated $Cp^*Rh(PMe_3)(\eta^2\text{-}C_6F_6)$. With strong evidence for the intramolecular route of eq 4. we conclude that $Cp^*Rh(PMe_3)$

Scheme V. Two Mechanisms for the Reaction of $CpIr(PMe_3)H_2$ with Hexafluorobenzene

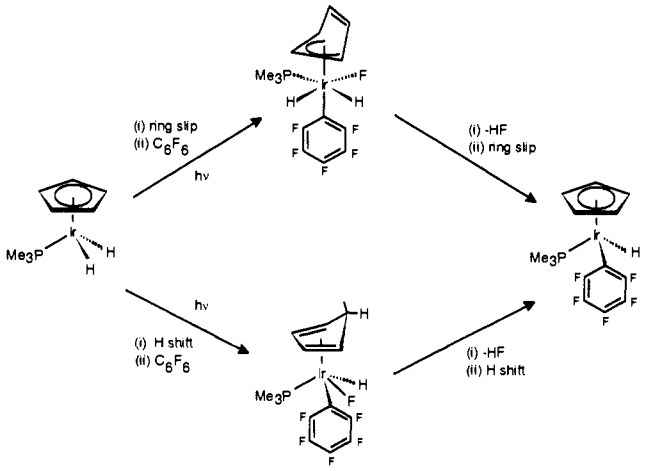

inserts into C–F bonds of C_6F_6 by the Parshall mechanism (eqs 3 and 4). with the modification that the second step must be photochemical. We have already secured strong evidence for the basic Parshall mechanism of benzene insertion both by isotopic labeling[29] and by laser flash photolysis.[10,55]

The matrix photochemistry reveals that both the CpRh and the Cp*Rh complexes of η^2-hexafluorobenzene react on irradiation in two ways, either to expel C_6F_6 or to insert into a C–F bond to form a (pentafluorophenyl)rhodium fluoride. The ratio of products is clearly dramatically different for the Cp and Cp* complexes. with a far larger proportion of C–F insertion in the Cp* case. The back reaction of C_6F_6 with $CpRh(PMe_3)$ in the matrix cage is probably prevented, not by cyclometalation, but by the reorganization of the C_6F_6 on coordination which generates a barrier to reaction. The ability of the matrix to accommodate ligand reorganization is also highlighted by the insertion reaction (compare the crystal structures of $CpRh(PMe_3)(\eta^2\text{-}C_6F_6)$ and $Cp^*Rh(PMe_3)(C_6F_5)Cl$). There are parallels between the matrix photochemistry of $CpRh(PMe_3)(C_2H_4)$[43] and that of $CpRh(PMe_3)(\eta^2\text{-}C_6F_6)$: intramolecular insertion competes with intermolecular substitution in a nitrogen matrix, but only substitution is observed in a CO matrix. However, it does not seem appropriate to postulate a similar mechanism with an in-cage reaction since we have not observed C–F activation in toluene glasses or by thermal reaction of $Cp^*Rh(PMe_3)(Ph)H$ with C_6F_6 (see above).

The photolysis of $CpIr(PMe_3)H_2$ in hexafluorobenzene generates $CpIr(PMe_3)(\eta^2\text{-}C_6F_6)$, an exact analogue of the $(\eta^5\text{-}C_5R_5)Rh(PMe_3)(\eta^2\text{-}C_6F_6)$ (R = H, Me) complexes. However, the C–F insertion reaction contrasts with the rhodium system in two significant ways: (i) the C–F insertion product is formed concurrently with the $\eta^2\text{-}C_6F_6$ complex, and (ii) the product is the (pentafluorophenyl)metal *hydride*.[56] There is no sign of the corresponding fluoride or chloride. The change of metal from rhodium to iridium has brought a change in reactivity and a change in mechanism. Deuterium labeling demonstrates that the hydride in the product derives from the hydride of the precursor. These observations exclude H_2 photodissociation, the typical reaction of complexes of this type. Two mechanisms can be put forward instead: ring slippage or metal-to-ring hydrogen transfer (Scheme V).[57] The first mechanism involves ring slippage to form

(50) Trudell, B. C.; Price, S. J. W. *Can. J. Chem.* **1979**, *57*, 2251. Turner, D. W.; Baker. C.; Baker. A. D.; Brundle, C. R. *Molecular Photoelectron Spectroscopy*; Wiley: London, 1970.

(51) Chowdhury, S.; Grimsrud. E. P.; Heinis, T.; Kebarle, P. *J. Am. Chem. Soc.* **1986**, *108*, 3630. Wentworth, W. E.; Limero, T.: Chen, E. C. N. *J. Phys. Chem.* **1987**, *91*. 241.

(52) Symons, M. C. R.; Selby, R. C.; Smith. I. G.; Bratt. S. W. *Chem. Phys. Lett.* **1977**, *48*, 100.

(53) Shchegoleva, L. N.; Bilks, I. I.; Schastnev, P. V. *Chem. Phys.* **1983**, *82*, 343.

(54) Parshall, G. W. *Acc. Chem. Res.* **1975**, *8*, 113.

(55) Whether we consider C–H or C–F oxidative addition of arenes, there may be other as yet unidentified reaction intermediates which lie between the $M(\eta^2\text{-arene})$ complex and the final product and at higher energy than either.

(56) The reaction of $Cp^*Ir(PMe_3)(c\text{-}C_6H_{11})H$ with C_6F_6 at 110–130 °C yields a mixture of products. the major constituent of which is $Cp^*Ir(PMe_3)(C_6F_5)H$. The source of the hydride ligand has not been established. Bergman, R. G.; Burger, P. Personal communication.

(57) (a) Berry, M.; Elmitt. K.; Green, M. L. H. *J. Chem. Soc., Dalton Trans.* **1979**, 1950. (b) Bloyce, P. E.; Rest, A. J.; Whitwell, I.: Graham. W. A. G.; Holmes-Smith, R. *J. Chem. Soc., Chem. Commun.* **1988**, 846. (c) Jones, W. D.; Chandler. V. L.; Selmeczy. A. D. *Organometallics* **1991**. *10*, 1577. Jones, W. D.; Maguire, J. A. *Organometallics* **1985**. *4*, 951.

(η^3-Cp)Ir(PMe_3)(C_6F_5)(F)H_2, which then loses HF with concomitant reversion of the ring to η^5-coordination to form CpIr(PMe_3)(C_6F_5)H. The second mechanism involves a hydride migration to the ring to form (η^4-C_5H_6)Ir(PMe_3)H, which inserts into a C–F bond of C_6F_6 to form (η^4-C_5H_6)Ir(PMe_3)(C_6F_5)(F)H. The elimination of HF leaves (η^4-C_5H_6)Ir(PMe_3)(C_6F_5), the hydride then migrates back onto the metal, and the ring rebinds η^5 to form CpIr(PMe_3)(C_6F_5)H. We cannot yet distinguish these mechanisms, nor can we exclude the participation of the radical anion, $[C_6F_6]^{\bullet-}$.

Both the rhodium and iridium reactions involve oxidative addition of C_6F_6, even though the steps differ. The energetics of these reactions are of great interest, although hard to define. There is a very large discrepancy in the value of $D[C_6F_5$–F] between the two determinations.[58] In a recent critical evaluation, a value of 646 kJ mol^{-1} was preferred.[59] If we accept this value, the extra strength of the C–F bond of C_6F_6 compared to the C–H bond of benzene, $[D[C_6F_5$–F] – $D[C_6H_5$–H]] is 186 kJ mol^{-1}. In the iridium system, hexafluorobenzene appears to insert into one of the possible reaction intermediates (η^3-C_5H_5)Ir(PMe_3)H_2 or (η^4-C_5H_6)Ir(PMe_3)H. If any η^2-C_6F_6 complex (*not* CpIr(PMe_3)(η^2-C_6F_6)) is involved in this process, it remains unobserved. The rhodium complex probably undergoes C–F insertion in the excited state of Cp*Rh(PMe_3)(η^2-C_6F_6). In that case the reaction not only involves cleavage of a very strong bond but also rearrangement of the C_6F_5 fragment. The extent of rearrangement can be visualized by contrasting the bond lengths and angles of the C_6F_6/C_6F_5 units of the two structures determined here. Of the many groups capable of undergoing oxidative addition to a transition metal center, the C–F bond must be one of the least reactive. Nevertheless, the strength of the C–F bond certainly does not provide an insuperable obstacle to reaction, at least in part because of the ability of C_6F_6 to coordinate to the metal before insertion.

The discovery of oxidative addition of arene C–H bonds was followed by analogous reactions for alkanes.[60] In recent work in this group, we have demonstrated that intramolecular coordination of aliphatic C–F bonds is significant in the chemistry of (dfepe)Cr(CO)$_3$ (dfepe = $(C_2F_5)_2PCH_2CH_2P(C_2F_5)_2$).[61] As yet, fluoroalkanes remain inert to oxidative addition.

Conclusions

Our investigations of the reactivity of half-sandwich complexes of rhodium and iridium toward hexafluorobenzene have established the ability of this ligand to coordinate to transition metals and to undergo oxidative addition. In the case of the Cp*Rh(PMe_3) complexes, we have established that the C–F insertion reaction proceeds via an isolable η^2-C_6F_6 complex to yield a (pentafluorophenyl)rhodium *fluoride*. This is a graphic example of the Parshall mechanism of an arene oxidative addition in which the (η^2-arene) intermediate is isolable, but here both steps are photoinduced. The two crystal structures reveal the reorganization inherent in the conversion of an η^2-arene complex to an (aryl)metal complex. In the η^2-C_6F_6 structure, two C–F bonds are bent out of the plane and the arene ring is far from being a regular hexagon. In the (aryl)metal fluoride, not only is one C–F bond broken but the C_6F_5 group is restored to a normal planar structure with a regular hexagonal ring. The structure of CpRh(PMe_3)(η^2-C_6F_6) also reveals a very close contact between one of the fluorine atoms bound to a coordinated carbon and a methyl group. NMR evidence indicates that this contact persists in solution (cf. CpIr(C_2H_4)(η^2-C_6F_6)). The C–F insertion reaction of the iridium complex, CpIr(PMe_3)H_2, yields the (pentafluorophenyl)iridium *hydride* via a different mechanism involving prior ring-slip or metal-ring hydrogen transfer.

The matrix studies show that both the Cp and Cp* complexes, (η^5-C_5R_5)Rh(PMe_3)(η^2-C_6F_6), may undergo photochemical C–F insertion or C_6F_6 dissociation, but the proportion of C–F insertion is far higher for the Cp* complex. Thus, they agree with the solution studies in showing that insertion is more favorable for the Cp* complex, but the distinction is not so pronounced. The origin of the difference between the reactivity in matrices and that in solution remains to be established.

These studies demonstrate how the oxidative addition of arenes may be arrested at the η^2-arene stage or may be swung toward oxidative addition by a change of ancillary ligands (C_5H_5 to C_5Me_5) or by a change of metal (rhodium to iridium). Parallel studies of polycyclic aromatics and of 1,4-$C_6H_4(CF_3)_2$ as ligands have shown how equilibria between η^2-arene and aryl hydride products may be achieved and how the equilibria may be controlled by choice of ancillary ligand, metal, and the arene itself.[62]

Acknowledgment. We are grateful to the Royal Society, British Gas, NATO, SERC. The Fulbright Foundation, and The EC Commission for support. We also acknowledge helpful discussions with Dr. S. B. Duckett and J. N. Hill. We appreciate the generosity of Prof. R. G. Bergman and Dr. P. Burger in revealing results prior to publication.

Supplementary Material Available: Tables of atomic coordinates, anisotropic thermal parameters, interatomic distances, bond angles, and least-squares planes (second structure only) (Tables VII–XIII) and packing diagrams (Figures 5 and 6) for the structures of CpRh(PMe_3)(η^2-C_6F_6) and Cp*Rh(PMe_3)(C_6F_5)Cl (12 pages). Ordering information is given on any current masthead page.

(58) Choo, K. Y.; Golden, D. M.; Benson, S. W. *Int. J. Chem. Kinet.* **1975**, *7*, 713. Krech, M. J.; Price, S. J. W.; Sapiano, H. J. *Can. J. Chem.* **1977**, *55*, 4222.

(59) Smart, B. E. *Mol. Struct. Energ.* **1986**, *3*, 141.

(60) (a) Janowicz, A. H.; Bergman, R. G. *J. Am. Chem. Soc.* **1982**, *104*, 352. (b) Hoyano, J. K.; Graham, W. A. G. *J. Am. Chem. Soc.* **1982**, *104*, 3723. (c) Janowicz, A. H.; Bergman, R. G. *J. Am. Chem. Soc.* **1983**, *105*, 3429.

(61) Brookhart, M.; Chandler, W.; Kessler, R. J.; Liu, Y.; Pienta, N.; Santini, C. C.; Hall, C.; Perutz, R. N.; Timney, J. A. *J. Am. Chem. Soc.* **1992**, *114*, 3802.

(62) Belt, S. T.; Dong, L.; Duckett, S. B.; Jones, W. D.; Partridge, M. G.; Perutz, R. N. *J. Chem. Soc., Chem. Commun.* **1991**, 266.